This article has been accepted for publication in a future issue of this journal, but has not been fully edited. Content may change prior to final publication. Citation information: DOI 10.1109/TVT.2020.3031662, IEEE Transactions on Vehicular Technology

Stability Region and Delay Analysis of a SWIPT-Based Two-Way Relay Network With Opportunistic Network Coding

Masoumeh Moradian, *Member, IEEE*, Farid Ashtiani, *Member, IEEE* and Ahmad Khonsari, *Member, IEEE*

***Abstract*—In this paper, we consider a buffer-aided two-way relay network in which a wireless-powered relay acts as an intermediate node for exchanging the data between two sources. The relay applies a time-switching (TS) policy to switch between data decoding (DD) and energy harvesting (EH) modes. Due to the presence of data queues at the relay, the relay is capable of employing opportunistic network coding (ONC) for transmission of the packets. Based on some realistic assumptions, we derive the stability region of such a network through designing TS and ONC policies. It is proved that the stability region is characterized by the TS policy and zero-wait ONC policy. Moreover, we derive the throughput-optimal and power-optimal policies and show that these policies provide the maximum coding opportunities. Also, we derive the average delay of an applied TS-ONC policy at the relay through modeling the data queues and energy buffer of the relay by two inter-related quasi-birth-death processes. We show that although waiting in ONC does not contribute to throughput-optimal and power-optimal policies, it can reduce the average delay. Finally, through simulation, we confirm our analytical results.**

***Index Terms*—Two-way relay network, Opportunistic network coding, SWIPT, Throughput, Delay, Quasi-birth-death process.**

I. Introduction

WIRELESS energy harvesting (WEH) has attracted a lot of attention in recent years since it enables the wireless nodes to prolong their lifetime through harvesting energy from radio frequency (RF) waves. WEH is especially an appropriate solution in Internet-of-things and machine-to-machine communications, where a large number of nodes should be powered up to communicate to each other [1]. In WEH, the wireless nodes can receive data and energy from the same RF signals. However, if a signal is exploited for data decoding (DD), then it cannot be reused for EH [2]. Two receiver architectures, based on time-switching (TS) and power-splitting (PS), have been proposed for simultaneous wireless transfer of power and information (SWIPT). In the TS architecture, the receiver switches in time between DD and EH modes, while in the PS one, it uses a fraction of the received RF power for DD and the rest for EH. SWIPT is an appealing choice in relay networks, where the sources can power up their desired relays through SWIPT. In this regard, optimal TS and PS relaying protocols have been extensively studied in different SWIPT-based one-way relaying scenarios, e.g., full-duplex, MIMO, and OFDM relaying systems [3]–[5].

On the other hand, two-way relay networks (TWRNs) have been studied extensively in the literature. The incorporation of network coding in TWRNs improves the spectral efficiency as well as the power consumption significantly by enabling the relay to transmit a coded version of the data of two sources at one slot, instead of transmitting each data separately [6]. The performance of different NC protocols, based on decode-and-forward (DF) and amplify-and-forward (AF), have been well studied in non-EH TWRNs [7], [8]. Moreover, in buffer-aided (or queue-aided) TWRNs, the relay is also capable of applying opportunistic network coding (ONC), i.e., to decide whether to send the uncoded data of one source or wait for a coding opportunity, which is provided when the data of the other source is available. In non-EH TWRNs, the employment of ONC results in a tradeoff between the power consumption and average delay of the packets [9]. More precisely, waiting in ONC decreases the power consumption through increasing the network-coded transmissions but increases the average delay due to not transmitting the data immediately. Furthermore, the effects of ONC on power, delay, and stability region have been shown in non-EH relays in which the energy is always available. However, in a WEH relay, the energy is intermittently available and its dynamic is affected by the wireless transmissions used for EH. Thus, it is interesting to investigate the effects that ONC can have in queue-aided TWRNs with a WEH relay.

SWIPT-based TWRNs were studied in [10]–[14]. In [10], the optimal PS ratio at a DF relay of a TWRN is derived to maximize the achievable sum rate. The authors in [11] propose a dynamic PS scheme to minimize the outage probability in a TWRN with a WEH DF relay. The authors in [12] investigate the outage probability and throughput of a WEH TWRN, where the sources have multiple antennas and the WEH relay uses TS protocol and analog NC. In [13], in addition to TS and PS relaying parameters, the durations of the uplink and downlink transmission of the source and relay, i.e., multiple access and broadcast phases, respectively, are optimized in order to minimize the outage probability of a WEH DF relay. In [14], the authors analyze the throughput of a TWRN by considering the PS scheme as well as DF and AF relaying methods. The problem of relay selection in SWIPT-based TWRNs is considered in [15], where the authors propose learning-based neural networks for relay selection in a TWRN with cognitive relays. While most works consider perfect

M. Moradian and A. Khonsari are with the School of Computer Science, Institute for Research in Fundamental Sciences (IPM), Teharn, Iran. F. Ashtiani is with the Department of Electrical Engineering, Advanced Communications Research Institute (ACRI), Sharif University of Technology, Tehran, Iran (email: mmoradian@ipm.ir, ashtianimt@sharif.edu, ak@ipm.ir.).

channel state information (CSI), the authors in [16] consider imperfect CSI when designing the precoders and PS scheme in a MIMO TWRN. The aforementioned studies, analyze and optimize the TWRN performance from a physical layer perspective. In particular, they do not consider energy storage or data queues at the relay. The energy storage improves the performance of EH nodes by reducing the degrading effects of the random nature of the energy harvesting. Moreover, the data queues provide the possibility of not dropping the unsuccessfully transmitted packets, by storing them for a retransmission in the future. In this regard, in SWIPT-based relays with TS architecture, the data queues lead to saving the time that should be spent for receiving the data again.

The scenarios in [17]–[19] consider data queues in the EH relay of a TWRN. In [17], the authors consider a relay node in a multihop network, with two separate data queues for exchanging the information between two sources. The relay performs ONC and harvests energy from non-RF energy resources. A multi-timescale model is proposed to strike the balance between availability of the energy and latency of the packets at the relay. In [18], the performance of digital and physical NC schemes are investigated in a three-node EH TWRN, where energy can be transferred from the relay to the sources independent from data transmissions. The authors in [19] consider a queue-aided TWRN with SWIPT, where the relay has one energy buffer and two data queues. The relay chooses one of EH, multiple access, or broadcast modes in each slot, where it harvests energy from both sources in the first mode, decodes the data of both sources in the second mode, and broadcasts a coded message to both sources in the third mode. Thus, the sources are coordinated. With the knowledge of complete system state, the mode selection policy and transmission powers and rates of the nodes are optimized to maximize the achievable rate region and derive an adaptive delay-aware scheduling algorithm. Regarding an information-theoretic point of view in [19] as well as knowing complete CSI, there is not any error in transmissions. Moreover, the authors follow a dynamic optimization approach, where the transmission mode and transmission power and rate of the nodes change in each slot adaptively to the network state, including the channel states. However, in our paper, we assume that only the statistics of the channels are known. Thus, regarding these statistics, we assume some probability of error for each transmission. Accordingly, the static TS and ONC policies are optimized at the relay to achieve the desired metrics. Also, due to considering error probabilities for the channels as well as non-coordinated sources, we have random arrivals at data queues and energy buffer of the relay. Consequently, unlink [19], queueing analysis is proposed for deriving the stability region and average delay.

In this paper, we focus on a SWIPT-based TWRN with two sources and a WEH DF relay, equipped with two data queues and an energy buffer. The relay is supposed to exchange specific data arrival rates between the sources. In order to receive data and energy from sources, the relay uses static TS policies to switch between the DD and EH modes. Moreover, in order to avoid excess energy transfer to the relay, the sources transmit randomly and adapt their transmission probabilities according to the relay TS policy and the data arrival rates to be exchanged. Due to having data queues at the relay and random transmissions of the sources, the relay is capable of applying ONC policy for transmitting the packets in coded form. The relay chooses TS and ONC policies in order to stabilize its data queues, which leads to the successful exchange of specified data arrival rates between the sources. While preserving the stability, the TS and ONC policies can also be determined to achieve the throughput, power, and delay optimality in the network. Our main contributions are listed as in the following:

- In a queue-aided SWIPT-based TWRN with random transmissions of the sources, we investigate the design of static TS and ONC policies to derive the stability region of the network. The stability region indicates the successful data arrival rates that can be exchanged between the sources successfully. Considering some realistic assumptions on the amount of harvested energy, we derive the stability region and show that by employing zero-wait ONC policy and choosing a suitable TS policy, we can achieve any arbitrary point in the stability region, i.e., waiting in ONC policy does not contribute to the stability of the network.
- In the considered network scenario, we derive the throughput-optimal and power-optimal policies. The power-optimal policy is defined as the policy that minimizes the transferred power by the sources, while preserving the stability of the queues. We show that the throughput-optimal and power-optimal TS policies lead to maximum possible NC opportunities in essence, and thus, waiting in ONC is not helpful.
- We derive the average delay of the considered network scenario, associated to arbitrary TS and ONC policies at the relay through modeling the data queues and energy buffer by two inter-related quasi-birth-death (QBD) processes and solving them iteratively. Then, we show that unlike the case of non-EH TWRNs, the delay-optimal ONC policy in WEH TWRNs may wait for a coding opportunity.

The paper is organized as follows. Section II introduces the network scenario. In Section III, the stability region of the network is derived. Section IV proposes throughput-optimal and power-optimal policies. In Section V, we derive the average delay by modeling the data and energy queues at the relay through inter-related QBDs. Numerical results are presented in Section VI to validate our analytical approach. Finally, Section VII concludes the paper.

II. System Model

We consider a TWRN which consists of one relay node, denoted by R, and two source nodes, denoted by S_1 and S_2, as shown in Fig. 1. There is no direct link between the sources and they communicate with each other through node R. Moreover, the sources have external power supplies and transmit their data as fixed-size packets to node R. However, node R is a WEH node which harvests energy from RF transmissions of nodes S_1 and S_2, and stores the harvested energy in a finite-size rechargeable energy buffer (battery),

This article has been accepted for publication in a future issue of this journal, but has not been fully edited. Content may change prior to final publication. Citation information: DOI 10.1109/TVT.2020.3031662, IEEE Transactions on Vehicular Technology

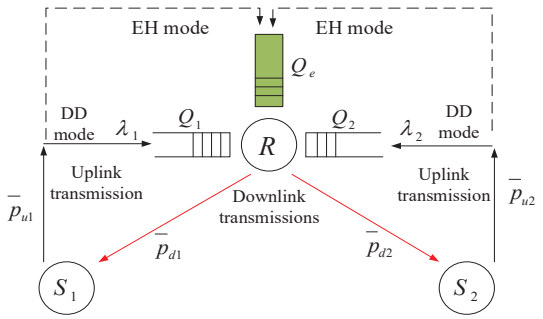

Fig. 1. Network scenario.

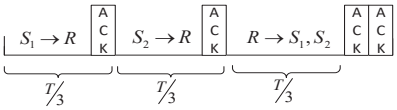

Fig. 2. The structure of a time slot.

denoted by Q_e. Also, node R stores the decoded data packets of nodes S_1 and S_2 in the data buffers Q_1 and Q_2, respectively. Note that the packets in Q_i ($i \in \{1,2\}$) are destined for S_j ($j \neq i$). For the sake of stability analysis, Q_1 and Q_2 are assumed to have infinite capacities (that is, sufficiently large in practice) [9], [19]. In the following, we express our assumptions on the timing and channel models, uplink and downlink communications, and EH profile, respectively. Notations used in our work, are listed in Table I.

A. Timing and channel models

Time is slotted in our scenario. Each time slot is considered as the time unit and is divided into three subslots, as shown in Fig. 2. Moreover, the duration of each subslot is equal to one packet transmission time. The first and second subslots in each slot are dedicated to the uplink transmissions, i.e., transmissions from nodes S_1 and S_2 to node R, respectively. In the third subslot, node R broadcasts to nodes S_1 and S_2.

We assume block fading channels, i.e., the channel gains remain constant during a subslot. Also, all channels in our scenario, including the uplink ones, denoted by S_i-R ($i \in \{1,2\}$), and the downlink ones, denoted by R-S_i ($i \in \{1,2\}$), are independent from each other along the time. Furthermore, each channel is independently and identically distributed across different subslots and follows a practical distribution, e.g., Nakagami. We assume that node R is not aware of the channel states and thus, the TS and ONC policies are designed at node R based on the average detection probabilities in different communication channels. In this regard, $\bar{p}_{ui}$ and $\bar{p}_{di}$ ($i \in \{1,2\}$) denote the average detection probabilities of the uplink and downlink channels S_i-R and R-S_i, respectively. Note that $\bar{p}_{ui}$ and $\bar{p}_{di}$ depend on the physical parameters of the system, e.g., the transmission power of the sources and relay, noise power, the statistics of the channel gains, modulation scheme, etc.

B. Uplink Communication Scheme

In order to receive data and harvest energy form source transmissions, node R applies static TS policies in the uplink subslots. In particular, it switches to the DD mode at the beginning of the first and second subslots of each slot with probabilities α_1 and α_2, and to the EH mode with probabilities $1-\alpha_1$ and $1-\alpha_2$, respectively. When operating in the EH mode in subslot i ($i \in \{1,2\}$), node R harvests energy from the transmission of node S_i (if any) and stores the harvested energy in Q_e. However, when operating in the DD mode, it decodes the transmitted packet of node S_i (if any) and then, in the case of successful decoding, stores the decoded packet in Q_i and sends an ACK to node S_i. Consequently, node S_i discards the transmitted packet from its queue and generates the next new packet immediately. However, if no ACK is received, node S_i keeps the packet for a retransmission. Thus, the sources have always a packet to transmit.

On the other hand, the relay is supposed to exchange the specified data rates λ_1 and λ_2 from node S_1 to node S_2 and vice verse, respectively. To this end, node R should choose the TS policy α_i ($i \in \{1,2\}$) such that the arrival rate to Q_i

TABLE I
NOTATIONS

Notation	Explanation
Q_1 (Q_2)	Data buffer for the packets of node S_1 (S_2)
Q_e	Energy buffer at node R
q_1 (q_2)	The number of data packets backlogged at Q_1 (Q_2)
q_e	The number of energy units backlogged at Q_e
N	Size of the energy buffer, Q_e
K	The number of energy units used for a packet transmission at node R
$\bar{p}_{u1}$ ($\bar{p}_{u2}$)	Average detection probability of the uplink channel S_1-R (S_2-R)
$\bar{p}_{d1}$ ($\bar{p}_{d2}$)	Average detection probability of the downlink channel $R-S_1$ ($R-S_2$)
$f_1(m)$ ($f_2(m)$)	The probability of harvesting m energy units from a transmission of node S_1 (S_2)
$a^{\max}$	The maximum number of energy units that can be harvested in a single slot
$\bar{e}_1$ ($\bar{e}_2$)	The average number of energy units harvested from a transmission of node S_1 (S_2)
α_1 (α_2)	The probability of switching to the DD mode in the first (second) subslot
β_1 (β_2)	The probability of transmitting a packet at node R when only Q_1 (Q_2) is non-empty
$\boldsymbol{\alpha}=(\alpha_1,\alpha_2)$	The TS policy at node R
$\boldsymbol{\beta}=(\beta_1,\beta_2)$	The ONC policy at node R
λ_1 (λ_2)	The data arrival rate at Q_1 (Q_2)
r_1 (r_2)	The packet transmission probability at node S_1 (S_2)
λ_{o1} (λ_{o2})	The total departure rate at Q_1 (Q_2)
μ_1^{-1} (μ_2^{-1})	The average transmission attempt time at Q_1 (Q_2)
λ_c	The coded transmission rate at node R
γ_H	The EH rate at node R
γ_C	The energy consumption rate at node R
p_b	The energy blockage probability at Q_e
ν ($\check{\nu}$)	The queue with maximum (minimum) total arrival rate
$\mathcal{R}$	Stability region
$\partial\mathcal{R}$	The border of the stability region
$\Pi_{\boldsymbol{\lambda}=(\lambda_1,\lambda_2)}$	The set of stabilizing policies at node R
$\boldsymbol{\lambda}^{\text{Th}}$	The throughput-optimal data arrival rate pair
$\Pi_{\boldsymbol{\lambda}}^{\text{PO}}$	The set of power-optimal policies at $\boldsymbol{\lambda}$
τ_{avg}	Average transmission delay of the source packets at node R

becomes λ_i. Then, by assuming that node S_i transmits one packet in each subslot i with probability one, α_i should satisfy $\lambda_i = \alpha_i \bar{p}_{\mathrm{u}i}$ since any packet transmitted by node S_i is decoded at node R with probability α_i and its decoding is successful with probability $\bar{p}_{\mathrm{u}i}$. However, transmitting with probability one in each slot may lead to excess power consumption at node S_i. In this regard, we assume that node S_i transmits a packet in each slot with probability r_i. Then, r_i and α_i should satisfy $\lambda_i = r_i \alpha_i \bar{p}_{\mathrm{u}i}$, leading to

$$r_i = \frac{\lambda_i}{\alpha_i \bar{p}_{\mathrm{u}i}}, \quad \frac{\lambda_i}{\bar{p}_{\mathrm{u}i}} \leq \alpha_i \leq 1, \quad i \in \{1,2\}. \tag{1}$$

where the inequality in (1) is resulted from $r_i = \frac{\lambda_i}{\alpha_i \bar{p}_{\mathrm{u}i}} \leq 1$ and $\alpha_i \leq 1$. As can be seen from (1), to support data arrival rate λ_i at node R, any α_i satisfying $\frac{\lambda_i}{\bar{p}_{\mathrm{u}i}} \leq \alpha_i \leq 1$ can be chosen, where each α_i indicates a specific r_i. However, along with supporting the data arrival rates λ_1 and λ_2, the values of α_1 and α_2 should be chosen such that a desired performance criterion, e.g., stability of the network, maximum throughput or minimum energy transferred by the sources, is achieved. It is also worth mentioning that multiple values of (α_1, α_2) may yield the considered performance criterion. Once α_i ($i \in \{1,2\}$) is determined at node R, node S_i adapts its transmission probability r_i according to (1). To derive r_i, the source becomes aware of the value of $\alpha_i \bar{p}_{\mathrm{u}i}$ through ACK messages.

C. Downlink Communication Scheme

We assume that the transmission power of node R is fixed. Thus, node R can transmit in the third subslot whenever the energy required for a packet transmission is available at Q_{e} and also, there exists at least one data packet at either Q_1 or Q_2. The transmission strategy of node R in the third subslot, i.e., transmitting a single packet, a network-coded packet, or not to transmit, is indicated by the ONC policy. In particular, according to the ONC policy, when both data queues are non-empty, node R transmits a coded packet generated by bit-wise XORing between the head-of-line (HoL) packets at Q_1 and Q_2 with probability one. On the other hand, when only Q_i ($i \in \{1,2\}$) is nonempty, node R transmits the HoL packet at Q_i with probability β_i, and does not transmit with probability $1-\beta_i$. In fact, in the latter case, node R randomly waits a slot for a coding opportunity, i.e., a packet arrival in the other queue. After node R transmits a packet, either uncoded or coded, it waits for the ACK message(s) from the corresponding destination(s). If an ACK is received from node S_i ($i \in \{1,2\}$), node R removes the head-of-line packet from Q_j ($j \neq i$) (note that the packets in Q_j are destined for S_i ($i \neq j$)). Otherwise, it keeps the packet for retransmission in the following slots. In the sequel, we represent a TS-ONC policy at node R by $((\alpha_1, \alpha_2), (\beta_1, \beta_2))$, where (α_1, α_2) and (β_1, β_2) represent the TS and ONC policies, respectively.

D. EH Profile

As mentioned before, when node R is in the EH mode, it harvests energy from the packet transmitted by node S_i in subslot i ($i \in \{1,2\}$) and then, stores the harvested energy in Q_{e}. The energy harvested in each slot is a continuous variable, however, due to our queueing analysis, we assume that node R harvests energy in discrete amounts, called energy units [20]. In this regard, we denote by $f_i(m)$ ($i \in \{1,2\}$), as the probability that node R harvests m energy units from a packet transmitted by node S_i. Note that $f_i(.)$ depends on physical system parameters, e.g., transmission power of node S_i, statistics of the gain of channel S_i-R, distance between nodes R and S_i, etc. Since our analysis is based on $f_i(.)$, we consider the related physical system parameters in Section VI, where we discretize a continuous EH profile to derive $f_i(.)$.

Let $f(m)$ denote the probability of harvesting m energy units in a slot assuming that node R is in the EH mode in both uplink subslots. Then, we have $f(m) = \sum_{l=0}^{m} f_1(l) f_2(m-l)$. Moreover, define $a^{\max}$ as the minimum m such that $F(m) \geq 1-\delta$, where $F(m) = \sum_{l=0}^{m} f(l)$ and δ is a constant close to zero, e.g., $\delta = 0.001$. In fact, the probability of harvesting more than $a^{\max}$ energy units in a slot is very small. In this regard, we assume that $f(m) = 0$ for $m > a^{\max}$, i.e., at most $a^{\max}$ energy units can be harvested in a slot. Moreover, we consider scenarios in which setting the relay power less than $a^{\max}$ energy units per packet transmission results in very poor transmission quality and thus, is not practical, i.e., we have $K \geq a^{\max}$, where K denotes the number of consumed energy units per packet transmission. Finally, we assume that $N \geq 2K$, where N denotes the size of energy buffer in terms of energy units, i.e., node R can store the energy required for at least two transmissions. The assumptions $K \geq a^{\max}$ and $N \geq 2K$ enables us to analytically derive the stability region, throughput-optimal and power-optimal policies. Our numerical results show that if the assumption $K \geq a^{\max}$ does not hold but the value of K does not result in very poor transmission quality, our analytical approach is still sufficiently accurate. Moreover, the two aforementioned assumptions are not required in Section V, where we analyze the average delay of the packets.

III. Stability Region

In this section, we derive the stability region of the proposed network scenario. The stability region is the set of all data arrival rates (λ_1, λ_2) that can be exchanged between the sources via the relay. On the one hand, as noted in Section II-B, λ_1 and λ_2 are the data arrival rates at Q_1 and Q_2, respectively. On the other hand, Q_1 and Q_2 can deliver all their arrived packets to the corresponding destinations when they are stable. Therefore, (λ_1, λ_2) belongs to the stability region of the network, only if Q_1 and Q_2 can be stabilized under a TS-ONC policy. Thus, for deriving the stability region, we need to investigate the stability of the data queues under different TS-ONC policies. For this purpose, in the following, we first give the formal definitions of stability of a single queue and stability region of the proposed network.

A. Definitions

Definition 1: Let a_{avg}, b_{avg}, and c_{avg} denote the arrival, service[1], and departure rates at a data queue, respectively.

[1]The service rate is the inverse of the service time. The service time is defined as the average time required to transmit the HoL packet at the queue successfully.

Then, under some mild assumptions, the data queue is (mean-rate) stable if and only if $a_{\text{avg}} \leq b_{\text{avg}}$, or equivalently, $a_{\text{avg}} = c_{\text{avg}}$. Moreover, the data queue is at stability edge if and only if $a_{\text{avg}} = b_{\text{avg}}$ [22].

Let us denote by $\frac{1}{\mu_i}$ as the average time it takes to transmit the HoL packet at Q_i once, whether successful or not. Note that $\frac{1}{\mu_i}$ includes the probable waiting time for harvesting enough energy as well as a single slot for the packet transmission and thus, $\frac{1}{\mu_i} \geq 1$. Then, the service time at Q_i is written as $\frac{1}{\bar{p}_{\text{d}j}\mu_i}$ since each packet is transmitted $\frac{1}{\bar{p}_{\text{d}j}}$ times on average to be successfully received at node S_j. Consequently, the service rate at Q_i is equal to $\bar{p}_{\text{d}j}\mu_i$. On the other hand, we define $\lambda_{\text{o}i}$ as the total departure rate at node R, i.e., the rate of transmission attempts. Then, the real departure rate at Q_i is equal to $\bar{p}_{\text{d}j}\lambda_{\text{o}i}$ since each transmission is successful with probability $\bar{p}_{\text{d}j}$. Thus, regarding that λ_i, $\bar{p}_{\text{d}j}\mu_i$, and $\bar{p}_{\text{d}j}\lambda_{\text{o}i}$ are the arrival, service, and departure rates at Q_i, we restate Definition 1 for our network as in the following remark.

Remark 1: Q_i ($i \in \{1,2\}$) is stable if and only if $\frac{\lambda_i}{\bar{p}_{\text{d}j}} \leq \mu_i$, where $j \neq i$ and $j \in \{1,2\}$, or equivalently $\frac{\lambda_i}{\bar{p}_{\text{d}j}} = \lambda_{\text{o}i}$. Moreover, Q_i is at stability edge if and only if $\frac{\lambda_i}{\bar{p}_{\text{d}j}} = \mu_i$.

Definition 2: Let $\boldsymbol{\lambda} = (\lambda_1, \lambda_2)$, $\boldsymbol{\alpha} = (\alpha_1, \alpha_2)$, and $\boldsymbol{\beta} = (\beta_1, \beta_2)$. Then, the stability region of the proposed network is defined as

$$\begin{aligned}\mathcal{R} =\{&\boldsymbol{\lambda} \mid \exists\ (\boldsymbol{\alpha}, \boldsymbol{\beta}) \text{ such that for } i \in \{1,2\}: \\ &\frac{\lambda_i}{\bar{p}_{ui}} \leq \alpha_i \leq 1,\ 0 \leq \beta_i \leq 1,\ \text{Q}_i \text{ is stable.}\},\end{aligned} \tag{2}$$

where the inequality $\frac{\lambda_i}{\bar{p}_{ui}} \leq \alpha_i \leq 1$ is written based on (1). In fact, the stability region in (2) is the set of all $\boldsymbol{\lambda}$ for which there exists at least one TS-ONC policy that stabilizes the data queues at node R. It is worth noting that at a given $\boldsymbol{\lambda}$, multiple TS-ONC policies may result in the stability of node R, where the possibility of choosing multiple TS policies was explained in Section II-B. In this regard, we define $\Pi_{\boldsymbol{\lambda}}$ as the set of all stabilizing policies at $\boldsymbol{\lambda}$, i.e., we have

$$\begin{aligned}\Pi_{\boldsymbol{\lambda}} = \{(\boldsymbol{\alpha}, \boldsymbol{\beta}) \mid &\text{for } i \in \{1,2\}: \frac{\lambda_i}{\bar{p}_{ui}} \leq \alpha_i \leq 1, \\ &0 \leq \beta_i \leq 1,\ \text{Q}_i \text{ is stable at } \boldsymbol{\lambda}\}.\end{aligned} \tag{3}$$

Definition 3: Let $B^{\epsilon}_{\boldsymbol{\lambda}}$ be the closed ball (with its boundary) centered at $\boldsymbol{\lambda}$ with radius ϵ. Then, the border of stability region, denoted by $\partial\mathcal{R}$, is defined as ($\partial\mathcal{R} \subseteq \mathcal{R}$)

$$\partial\mathcal{R} = \{\boldsymbol{\lambda} \in \mathcal{R} \mid \forall\ \epsilon > 0\ : B^{\epsilon}_{\boldsymbol{\lambda}} \not\subset \mathcal{R}\} \tag{4}$$

Finally, we define ν and $\hat{\nu}$ as follows

$$\nu = \underset{\substack{i\in\{1,2\}\\ i\neq j}}{\arg\max} \frac{\lambda_i}{\bar{p}_{\text{d}j}}, \quad \hat{\nu} = \underset{\substack{i\in\{1,2\}\\ i\neq j}}{\arg\min} \frac{\lambda_i}{\bar{p}_{\text{d}j}}. \tag{5}$$

We refer to $\frac{\lambda_i}{\bar{p}_{\text{d}j}}$ as the total arrival rate at Q_i. Then, ν and $\hat{\nu}$ in (5) refer to the queues with maximum and minimum total arrival rates, respectively, and thus, are functions of $\boldsymbol{\lambda}$, i.e., $\nu = \nu(\boldsymbol{\lambda})$ and $\hat{\nu} = \hat{\nu}(\boldsymbol{\lambda})$. In the following, by proving some lemmas, we derive the stability region of the network.

B. Stability Region Analysis

We define γ_{H} as the EH rate at node R, i.e., the average number of energy units that are harvested at node R in a slot. Moreover, $\bar{e_i}$ denotes the average number of energy units that is harvested from a packet transmitted by node S_i in subslot i ($i \in \{1,2\}$), i.e., $\bar{e_i} = \sum_{m=0}^{a^{\max}} m f_i(m)$, where $f_i(.)$ is defined in Section II-D. Then, γ_{H} is derived as

$$\gamma_{\text{H}} = \gamma_{\text{H}}(\boldsymbol{\lambda}, \boldsymbol{\alpha}) = r_1(1-\alpha_1)\bar{e_1} + r_2(1-\alpha_2)\bar{e_2} \tag{6}$$

$$= \frac{1-\alpha_1}{\alpha_1\bar{p}_{\text{u}1}}\lambda_1\bar{e_1} + \frac{1-\alpha_2}{\alpha_2\bar{p}_{\text{u}2}}\lambda_2\bar{e_2},\ \frac{\lambda_i}{\bar{p}_{\text{u}i}} \leq \alpha_i \leq 1, i \in \{1,2\}. \tag{7}$$

The first and second terms in (6) indicate the EH rate at node R in the first and second subslots, respectively. Moreover, (7) is derived using (1). It indicates that γ_{H} is a function of $\boldsymbol{\lambda}$ and the TS policy, $\boldsymbol{\alpha}$, i.e., $\gamma_{\text{H}} = \gamma_{\text{H}}(\boldsymbol{\lambda}, \boldsymbol{\alpha})$. Let $\boldsymbol{\alpha}^*_{\boldsymbol{\lambda}}$ denote the TS policy which maximizes EH rate, γ_{H}, at a given $\boldsymbol{\lambda}$. Then, since from (7), γ_{H} is decreasing with α_i ($i \in \{1,2\}$) in the interval $\frac{\lambda_i}{\bar{p}_{\text{u}i}} \leq \alpha_i \leq 1$, its maximum is achieved at the minimum value of α_i, i.e., $\frac{\lambda_i}{\bar{p}_{\text{u}i}}$. Therefore, we have

$$\boldsymbol{\alpha}^*_{\boldsymbol{\lambda}} = \underset{i\in\{1,2\}:\ \frac{\lambda_i}{\bar{p}_{\text{u}i}} \leq \alpha_i \leq 1}{\arg\max} \gamma_{\text{H}}(\boldsymbol{\lambda}, \boldsymbol{\alpha}) = (\frac{\lambda_1}{\bar{p}_{\text{u}1}}, \frac{\lambda_2}{\bar{p}_{\text{u}2}}). \tag{8}$$

Note that $\boldsymbol{\alpha}^*_{\boldsymbol{\lambda}}$ results in $r_1 = r_2 = 1$, according to (1). Next, we define γ_{C} as the energy consumption rate at node R, i.e., the average number of energy units that are consumed at node R in a slot. γ_{C} is derived as

$$\gamma_{\text{C}} = K(\lambda_{\text{o}\nu} + \lambda_{\text{o}\hat{\nu}} - \lambda_{\text{c}}), \tag{9}$$

where λ_{c} is the rate of coded transmissions, whether successful or not. Eq. (9) is written considering that each departure at node R consumes K energy units, and that, the total departure rate at node R is $\lambda_{\text{o}\nu} + \lambda_{\text{o}\hat{\nu}} - \lambda_{\text{c}}$. Note that λ_{c} is subtracted from the total departure rates at the data queues, i.e., $\lambda_{\text{o}\nu} + \lambda_{\text{o}\hat{\nu}}$, since the coded transmissions are accounted two times in $\lambda_{\text{o}\nu} + \lambda_{\text{o}\hat{\nu}}$. It is worth noting that when both data queues are nonempty at the beginning of a downlink subslot and enough energy exists in Q_{e}, a coded transmission occurs with probability one. Thus, we have $\lambda_{\text{c}} = \Pr\{q_1 > 0, q_2 > 0, q_e \geq K\}$, where q_i ($i \in \{1,2\}$) and q_{e} denote the number of data packets and energy units in Q_i and Q_{e}, respectively, at the beginning of a downlink subslot. Therefore, λ_{c} depends on the joint distribution of q_1, q_2, and q_{e}, which is affected by the data arrival rates at the queues ($\boldsymbol{\lambda}$), EH rate ($\gamma_{\text{H}}(\boldsymbol{\lambda}, \boldsymbol{\alpha})$), and the service process of the packets. The last factor is affected by the ONC policy, $\boldsymbol{\beta}$. Thus, it can be concluded that λ_{c} and consequently, γ_{C} in (9), are functions of $\boldsymbol{\lambda}$, $\boldsymbol{\alpha}$, and $\boldsymbol{\beta}$, i.e., $\lambda_{\text{c}} = \lambda_{\text{c}}(\boldsymbol{\lambda}, \boldsymbol{\alpha}, \boldsymbol{\beta})$ and $\gamma_{\text{C}} = \gamma_{\text{C}}(\boldsymbol{\lambda}, \boldsymbol{\alpha}, \boldsymbol{\beta})$. However, throughout the paper, we drop the arguments, whenever they are clear from the context. Moreover, when $\boldsymbol{\lambda} \in \mathcal{R}$ and $(\boldsymbol{\alpha}, \boldsymbol{\beta}) \in \Pi_{\boldsymbol{\lambda}}$, by using Remark 1 and (9), we derive γ_{C} as follows

$$\gamma_{\text{C}} = K(\frac{\lambda_\nu}{\bar{p}_{\text{d}\hat{\nu}}} + \frac{\lambda_{\hat{\nu}}}{\bar{p}_{\text{d}\nu}} - \lambda_{\text{c}}). \tag{10}$$

Remark 2: In our scenario, the data queue Q_i ($i \in \{1,2\}$) can be modeled as a Geo/G/1 queue, i.e., a queue with geometric inter-arrival times (Geo), general service times (G),

This article has been accepted for publication in a future issue of this journal, but has not been fully edited. Content may change prior to final publication. Citation information: DOI 10.1109/TVT.2020.3031662, IEEE Transactions on Vehicular Technology

and one server. The packet inter-arrival times at Q_i follow a Geometric distribution since all processes affecting the arrival process at Q_i, including the transmissions of node S_i, TS policy at node R, and packet detection, are independent Bernoulli processes. A Geo/G/1 queue is always backlogged when it is at stability edge or unstable (refer to the P-K formula in [23]).

Using Remark 2, we introduce the the following lemma.

Lemma 1:

(a) If node R is unstable, then, Q_ν is unstable and $\gamma_{\mathrm{C}} = K\lambda_{\mathrm{o}\nu}$.

(b) If node R is stable and one of the queues is at stability edge, then, Q_ν is at stability edge and $\gamma_{\mathrm{C}} = K\frac{\lambda_\nu}{\bar{p}_{\mathrm{d}\hat{\nu}}}$.

Proof: See Appendix A. □

In either cases of Lemma 1, i.e., Q_ν being unstable or at stability edge, Q_ν is always backlogged, according to Remark 2, implying that all packets of $\mathrm{Q}_{\hat{\nu}}$ are transmitted in coded from. Then, $\lambda_{\mathrm{c}} = \lambda_{\mathrm{o}\hat{\nu}}$ and thus, from (9), $\gamma_{\mathrm{C}} = K\lambda_{\mathrm{o}\nu}$. When Q_ν is at stability edge, we further have $\lambda_{\mathrm{o}\nu} = \frac{\lambda_\nu}{\bar{p}_{\mathrm{d}\hat{\nu}}}$, according to Remark 1, which leads to $\gamma_{\mathrm{C}} = K\frac{\lambda_\nu}{\bar{p}_{\mathrm{d}\hat{\nu}}}$. It is worth to mention that node R, and consequently Q_ν according to Lemma 1, become unstable when either $\boldsymbol{\lambda} \notin \mathcal{R}$ or $\boldsymbol{\lambda} \in \mathcal{R}$ but the applied policy $(\boldsymbol{\alpha}, \boldsymbol{\beta}) \notin \Pi_{\boldsymbol{\lambda}}$. Moreover, Q_ν is at stability edge at any $\boldsymbol{\lambda} \in \mathcal{R}$ if $(\boldsymbol{\alpha}, \boldsymbol{\beta})$ satisfies the conditions in Lemma 4(b).

As noted before, the energy buffer Q_{e} is finite. Thus, part of γ_{H} might be wasted due to the limited capacity of Q_{e}. Let us define p_{b} as the energy blockage probability, i.e., the probability that an energy unit is blocked at Q_{e}. In the following lemma, using the assumptions $a^{\max} \leq K$ and $N \geq 2K$ (explained in Section II-D), we show that when Q_ν is always backlogged, p_{b} is zero if and only if zero-wait ONC policy is applied at Q_ν.

Lemma 2: If Q_ν is always backlogged, then $p_{\mathrm{b}} = 0$, or equivalently $\gamma_{\mathrm{C}} = \gamma_{\mathrm{H}}$, if and only if $\beta_\nu = 1$, i.e., zero-wait ONC is applied at Q_ν.

Proof: See Appendix B. □

Let us define $\mathcal{B}_{\boldsymbol{\lambda}} = \{\boldsymbol{\beta} \mid \beta_{\nu(\boldsymbol{\lambda})} = 1,\ \beta_{\hat{\nu}(\boldsymbol{\lambda})} \in [0,1]\}$. In fact, for $\boldsymbol{\beta} \in \mathcal{B}_{\boldsymbol{\lambda}}$, zero-wait ONC is applied at Q_ν, while it may or may not be applied at $\mathrm{Q}_{\hat{\nu}}$. We use Lemmas 1 and 2 to prove the following lemma.

Lemma 3:

(a) If $\exists(\boldsymbol{\alpha}, \boldsymbol{\beta}) \in \Pi_{\boldsymbol{\lambda}}$ (i.e., $\boldsymbol{\lambda} \in \mathcal{R}$), then $\gamma_{\mathrm{H}}(\boldsymbol{\lambda}, \boldsymbol{\alpha}) \geq K\frac{\lambda_\nu}{\bar{p}_{\mathrm{d}\hat{\nu}}}$.

(b) If $\gamma_{\mathrm{H}}(\boldsymbol{\lambda}, \boldsymbol{\alpha}) \geq K\frac{\lambda_\nu}{\bar{p}_{\mathrm{d}\hat{\nu}}}$, then $\{(\boldsymbol{\alpha}, \boldsymbol{\beta}) \mid \boldsymbol{\beta} \in \mathcal{B}_{\boldsymbol{\lambda}}\} \subseteq \Pi_{\boldsymbol{\lambda}}$, and, $\boldsymbol{\lambda} \in \mathcal{R}$.

Proof: See Appendix C. □

Lemma 3(a) states that if the TS-ONC policy $(\boldsymbol{\alpha}, \boldsymbol{\beta})$ is stabilizing at $\boldsymbol{\lambda}$, its corresponding EH rate should be greater than $K\frac{\lambda_\nu}{\bar{p}_{\mathrm{d}\hat{\nu}}}$. In fact, $K\frac{\lambda_\nu}{\bar{p}_{\mathrm{d}\hat{\nu}}}$ is the minimum possible energy consumption rate, which is achieved when $\lambda_{\mathrm{c}} = \frac{\lambda_{\hat{\nu}}}{\bar{p}_{\mathrm{d}\nu}}$ in (10), i.e., all packets of $\mathrm{Q}_{\hat{\nu}}$ are transmitted in coded form. Lemma 3(b) reveals that if the TS policy $\boldsymbol{\alpha}$ satisfies $\gamma_{\mathrm{H}}(\boldsymbol{\lambda}, \boldsymbol{\alpha}) \geq K\frac{\lambda_\nu}{\bar{p}_{\mathrm{d}\hat{\nu}}}$, the set of ONC policies which apply zero-wait ONC policy at Q_ν, but apply ONC at $\mathrm{Q}_{\hat{\nu}}$ arbitrarily are stabilizing. From Lemmas 3(a) and (b), we directly conclude the following corollary.

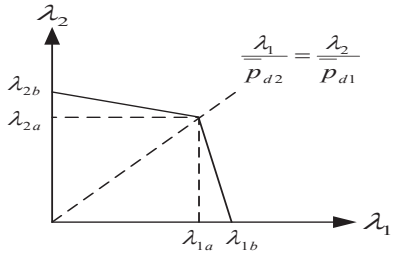

Fig. 3. Stability region of the static approach.

Corollary 1: $\boldsymbol{\lambda} \in \mathcal{R}$ if and only if there exists $\boldsymbol{\alpha}$ such that $\gamma_{\mathrm{H}}(\boldsymbol{\lambda}, \boldsymbol{\alpha}) \geq K\frac{\lambda_\nu}{\bar{p}_{\mathrm{d}\hat{\nu}}}$. Then, any $\boldsymbol{\beta} \in \mathcal{B}_{\boldsymbol{\lambda}}$, including $\boldsymbol{\beta} = (1,1)$, stabilizes node R. This reveals that waiting in ONC policy does not contribute to the stability of node R. In other words, if the TS policy satisfies $\gamma_{\mathrm{H}}(\boldsymbol{\lambda}, \boldsymbol{\alpha}) \geq K\frac{\lambda_\nu}{\bar{p}_{\mathrm{d}\hat{\nu}}}$, then node R is stabilized by applying zero-wait ONC policy. Otherwise, node R will not be stable under any ONC policy.

The stability region is derived in the following proposition.

Proposition 1: The stability region is derived as $\mathcal{R} = \{\boldsymbol{\lambda} | \gamma_{\mathrm{H}}(\boldsymbol{\lambda}, \boldsymbol{\alpha}^*_{\boldsymbol{\lambda}}) \geq K\frac{\lambda_\nu}{\bar{p}_{\mathrm{d}\hat{\nu}}}\}$, where $\boldsymbol{\alpha}^*_{\boldsymbol{\lambda}}$ is defined in (8).

Proof: Since $\boldsymbol{\alpha}^*_{\boldsymbol{\lambda}}$ maximizes $\gamma_{\mathrm{H}}(\boldsymbol{\lambda}, \boldsymbol{\alpha})$, we can find a TS policy satisfying $\gamma(\boldsymbol{\lambda}, \boldsymbol{\alpha}) \geq K\frac{\lambda_\nu}{\bar{p}_{\mathrm{d}\hat{\nu}}}$ if and only if $\gamma_{\mathrm{H}}(\boldsymbol{\lambda}, \boldsymbol{\alpha}^*_{\boldsymbol{\lambda}}) \geq K\frac{\lambda_\nu}{\bar{p}_{\mathrm{d}\hat{\nu}}}$. This fact, along with Corollary 1, proves the proposed relation for the stability region. □

Using (7) in Proposition 1, the stability region is written as

$$\mathcal{R} = \begin{cases} \lambda_1\left(\frac{K}{\bar{p}_{\mathrm{d}2}} + \frac{\bar{e_1}}{\bar{p}_{\mathrm{u}1}}\right) + \lambda_2\frac{\bar{e_2}}{\bar{p}_{\mathrm{u}2}} \leq \bar{e_1} + \bar{e_2}; & \frac{\lambda_1}{\bar{p}_{\mathrm{d}2}} \geq \frac{\lambda_2}{\bar{p}_{\mathrm{d}1}}, \\ \lambda_2\left(\frac{K}{\bar{p}_{\mathrm{d}1}} + \frac{\bar{e_2}}{\bar{p}_{\mathrm{u}2}}\right) + \lambda_1\frac{\bar{e_1}}{\bar{p}_{\mathrm{u}1}} \leq \bar{e_1} + \bar{e_2}; & \frac{\lambda_1}{\bar{p}_{\mathrm{d}2}} < \frac{\lambda_2}{\bar{p}_{\mathrm{d}1}}. \end{cases} \tag{11}$$

The stability region has been illustrated in Fig. 3. Moreover, $\lambda_{1\mathrm{a}}$, $\lambda_{1\mathrm{b}}$, $\lambda_{2\mathrm{a}}$, and $\lambda_{2\mathrm{b}}$ are derived as in the following:

$$\lambda_{1\mathrm{a}} = \frac{\bar{e_1} + \bar{e_2}}{\frac{K}{\bar{p}_{\mathrm{d}2}} + \frac{\bar{e_1}}{\bar{p}_{\mathrm{u}1}} + \frac{\bar{p}_{\mathrm{d}1}}{\bar{p}_{\mathrm{d}2}\bar{p}_{\mathrm{u}2}}\bar{e_2}}, \quad \lambda_{2a} = \frac{\bar{e_1} + \bar{e_2}}{\frac{K}{\bar{p}_{\mathrm{d}1}} + \frac{\bar{e_2}}{\bar{p}_{\mathrm{u}2}} + \frac{\bar{p}_{\mathrm{d}2}}{\bar{p}_{\mathrm{d}1}\bar{p}_{\mathrm{u}1}}\bar{e_1}},$$
$$\lambda_{1b} = \frac{\bar{e_1} + \bar{e_2}}{\frac{K}{\bar{p}_{\mathrm{d}2}} + \frac{\bar{e_1}}{\bar{p}_{\mathrm{u}1}}}, \quad \lambda_{2b} = \frac{\bar{e_1} + \bar{e_2}}{\frac{K}{\bar{p}_{\mathrm{d}1}} + \frac{\bar{e_2}}{\bar{p}_{\mathrm{u}2}}}. \tag{12}$$

Also, by some mathematical manipulation, it can be shown that the line connecting $(0, \lambda_{2b})$ and $(\lambda_{1b}, 0)$ lies below the border of stability region and thus, $\mathcal{R}$ is convex.

Although waiting in ONC does not contribute to the stability of node R, it may reduce the average delay of the packets, as will be seen in Section VI. A subset of stabilizing ONC policies at $\boldsymbol{\lambda} \in \mathcal{R}$ was shown to be $\mathcal{B}_{\boldsymbol{\lambda}}$, according to Corollary 1. The following lemma states that when $\gamma_{\mathrm{H}}(\boldsymbol{\lambda}, \boldsymbol{\alpha}) = K\frac{\lambda_\nu}{\bar{p}_{\mathrm{d}\hat{\nu}}}$, the only stabilizing ONC policies are $\boldsymbol{\beta} \in \mathcal{B}_{\boldsymbol{\lambda}}$, i.e., zero-wait ONC should be applied at Q_ν.

Lemma 4:

(a) If $\gamma_{\mathrm{H}}(\boldsymbol{\lambda}, \boldsymbol{\alpha}) = K\frac{\lambda_\nu}{\bar{p}_{\mathrm{d}\hat{\nu}}}$, then $(\boldsymbol{\alpha}, \boldsymbol{\beta}) \in \Pi_{\boldsymbol{\lambda}}$ if and only if $\boldsymbol{\beta} \in \mathcal{B}_{\boldsymbol{\lambda}}$.

(b) If $\gamma_{\mathrm{H}}(\boldsymbol{\lambda}, \boldsymbol{\alpha}) = K\frac{\lambda_\nu}{\bar{p}_{\mathrm{d}\hat{\nu}}}$ and $\boldsymbol{\beta} \in \mathcal{B}_{\boldsymbol{\lambda}}$, then Q_ν is at stability edge and thus, always backlogged.

Proof: See Appendix D. □

Corollary 2: When $\gamma_{\mathrm{H}}(\boldsymbol{\lambda}, \boldsymbol{\alpha}) = K\frac{\lambda_\nu}{\bar{p}_{\mathrm{d}\hat{\nu}}}$, we should have $\beta_\nu = 1$ to preserve the stability, according to Lemma 4(a). Then,

Q_ν becomes always backlogged, according to Lemma 4(b), implying that all packets of $\mathrm{Q}_{\hat{\nu}}$ are transmitted in coded form. Thus, waiting in ONC is irrelevant at $\mathrm{Q}_{\hat{\nu}}$. In this regard, when $\gamma_{\mathrm{H}}(\boldsymbol{\lambda},\boldsymbol{\alpha}) = K\frac{\lambda_\nu}{\bar{p}_{\mathrm{d}\hat{\nu}}}$, the stabilizing $\boldsymbol{\beta}$ is considered to be only $(1,1)$.

Corollary 3: From Proposition 1, and by considering Definition 3, the border of stability region is indicated as $\partial\mathcal{R} = \{\boldsymbol{\lambda}|\gamma_{\mathrm{H}}(\boldsymbol{\lambda},\boldsymbol{\alpha}^*_{\boldsymbol{\lambda}}) = K\frac{\lambda_\nu}{\bar{p}_{\mathrm{d}\hat{\nu}}}\}$. Then, using Corollary 2, Q_ν is always backlogged at $\boldsymbol{\lambda}\in\partial\mathcal{R}$. Moreover, $\Pi_{\boldsymbol{\lambda}} = (\boldsymbol{\alpha}^*_{\boldsymbol{\lambda}},(1,1))$. This is due to the fact that on the one hand, at $\boldsymbol{\alpha}^*_{\boldsymbol{\lambda}}$, the only stabilizing $\boldsymbol{\beta}$ is $(1,1)$, according to Corollary 2. On the other hand, no other policy with $\boldsymbol{\alpha}\neq\boldsymbol{\alpha}^*_{\boldsymbol{\lambda}}$ can belong to $\Pi_{\boldsymbol{\lambda}}$ since using (8) and $\gamma_{\mathrm{H}}(\boldsymbol{\lambda},\boldsymbol{\alpha}^*_{\boldsymbol{\lambda}}) = K\frac{\lambda_\nu}{\bar{p}_{\mathrm{d}\hat{\nu}}}$, such a policy satisfies $\gamma_{\mathrm{H}}(\boldsymbol{\lambda},\boldsymbol{\alpha}) < \gamma_{\mathrm{H}}(\boldsymbol{\lambda},\boldsymbol{\alpha}^*_{\boldsymbol{\lambda}}) = K\frac{\lambda_\nu}{\bar{p}_{\mathrm{d}\hat{\nu}}}$ and thus, is not stabilizing according to Lemma 3(a).

IV. Throughput-optimal and Power-optimal Policies

A. Throughput-Optimal Policy

The throughput of the network is defined as the successful data rates exchanged between nodes S_1 and S_2, i.e., $\lambda_1+\lambda_2$, given that node R is stable. In the following proposition, we derive the throughput-optimal policy.

Proposition 2: In the considered TWRN, the throughput-optimal policy is $(\boldsymbol{\alpha}^*_{\boldsymbol{\lambda}^{\mathrm{Th}}},(1,1))$, where $\boldsymbol{\alpha}^*_{\boldsymbol{\lambda}}$ is given in (8). Also, $\boldsymbol{\lambda}^{\mathrm{Th}}\in\partial\mathcal{R}$ and is derived as

$$\boldsymbol{\lambda}^{\mathrm{Th}} = \begin{cases} (\lambda_{1\mathrm{a}},\lambda_{2\mathrm{a}}); & \frac{\bar{e}_1}{\bar{p}_{\mathrm{u}1}} - \frac{\bar{e}_2}{\bar{p}_{\mathrm{u}2}} \le \frac{K}{\bar{p}_{\mathrm{d}2}},\ \frac{\bar{e}_2}{\bar{p}_{\mathrm{u}2}} - \frac{\bar{e}_1}{\bar{p}_{\mathrm{u}1}} \le \frac{K}{\bar{p}_{\mathrm{d}1}},\\ (\lambda_{1\mathrm{b}},0); & \frac{\bar{e}_1}{\bar{p}_{\mathrm{u}1}} - \frac{\bar{e}_2}{\bar{p}_{\mathrm{u}2}} > \frac{K}{\bar{p}_{\mathrm{d}2}},\\ (0,\lambda_{2\mathrm{b}}); & \frac{\bar{e}_2}{\bar{p}_{\mathrm{u}2}} - \frac{\bar{e}_1}{\bar{p}_{\mathrm{u}1}} > \frac{K}{\bar{p}_{\mathrm{d}1}}, \end{cases} \tag{13}$$

where $\lambda_{1\mathrm{a}}$, $\lambda_{2\mathrm{a}}$, $\lambda_{1\mathrm{b}}$, and $\lambda_{2\mathrm{b}}$ are given in (12).

Proof: The throughput, $\lambda_1+\lambda_2$, is maximized at one of the corners of the stability region since the stability region, shown in Fig. 3, is convex. Thus, it is enough to compare the throughput at points $(\lambda_{1\mathrm{a}},\lambda_{2\mathrm{a}})$, $(0,\lambda_{2\mathrm{b}})$, and $(\lambda_{1\mathrm{b}},0)$, which are $\lambda_{1\mathrm{a}}+\lambda_{2\mathrm{a}}$, $\lambda_{2\mathrm{b}}$, and $\lambda_{1\mathrm{b}}$, respectively. By using (12) and some mathematical manipulation, the throughput-optimal $\boldsymbol{\lambda}$, denoted by $\boldsymbol{\lambda}^{\mathrm{Th}}$, is derived as in (13). Moreover, since $\boldsymbol{\lambda}^{\mathrm{Th}}$ belongs to $\partial\mathcal{R}$, Q_ν is always backlogged and we have $\Pi_{\boldsymbol{\lambda}^{\mathrm{Th}}} = (\boldsymbol{\alpha}^*_{\boldsymbol{\lambda}^{\mathrm{Th}}},(1,1))$, according to Corollary 3. Also, using the assumption $K\ge a^{\max}$, we have $|\bar{e}_1-\bar{e}_2|\le K$. Then, if $\bar{p}_{\mathrm{u}i} > \bar{p}_{\mathrm{d}j}$ for $i,j\in\{1,2\}$, the constraints of the first case in (13) hold and thus, the throughput-optimal policy is a two-way relaying policy. □

B. Power-Optimal policy

In this part, we aim to minimize the energy transferred by the sources to the relay through minimizing the EH rate, γ_{H}, at node R. In this regard, a power-optimal policy at $\boldsymbol{\lambda}\in\mathcal{R}$ is defined as the policy that minimizes the EH rate, given that the stability of node R is preserved. In fact, the power-optimal policy is the answer of the following optimization

$$\underset{(\boldsymbol{\alpha},\boldsymbol{\beta})\in\Pi_{\boldsymbol{\lambda}}}{\arg\min}\ \gamma_{\mathrm{H}}(\boldsymbol{\lambda},\boldsymbol{\alpha}) \tag{14}$$

In the following proposition, we derive the power-optimal policies at $\boldsymbol{\lambda}\in\mathcal{R}$ and show that under such policies, the energy consumption rate at node R is minimized and no energy is wasted (blocked). Since the energy consumed or wasted at node R is supplied by the sources, minimizing γ_{H} is tantamount to minimizing energy consumption at the sources. If the sources are some sensors, regarding battery capacity in the sensors, it prolongs the lifetime of those sensor nodes.

Proposition 3: The set of power-optimal TS policies at $\boldsymbol{\lambda}\in\mathcal{R}$ is $\Pi^{\mathrm{PO}}_{\boldsymbol{\lambda}} = \{(\boldsymbol{\alpha},(1,1))|\gamma_{\mathrm{H}}(\boldsymbol{\lambda},\boldsymbol{\alpha}) = K\frac{\lambda_\nu}{\bar{p}_{\mathrm{d}\hat{\nu}}}\}$. Moreover, under a power-optimal TS policy, Q_ν is at stability edge. Also, the power-optimal TS policy, (α_1,α_2), satisfies the following relations

$$\frac{1}{\min\{\frac{\bar{p}_{\mathrm{u}1}}{\lambda_1},g^{-1}(1)\}} \le \alpha_1 \le \frac{1}{\max\{g^{-1}(\frac{\bar{p}_{\mathrm{u}2}}{\lambda_2}),1\}},\ \alpha_2 = \frac{1}{g(\frac{1}{\alpha_1})},$$
$$g(x) = 1+\frac{\bar{p}_{\mathrm{u}2}}{\lambda_2\bar{e}_2}[K\frac{\lambda_\nu}{\bar{p}_{\mathrm{d}\nu}} - \frac{\lambda_1\bar{e}_1}{\bar{p}_{\mathrm{u}1}}(x-1)]. \tag{15}$$

Proof: According to Lemma 3(a), we have $\gamma_{\mathrm{H}}(\boldsymbol{\lambda},\boldsymbol{\alpha})\ge K\frac{\lambda_\nu}{\bar{p}_{\mathrm{d}\hat{\nu}}}$ for any $(\boldsymbol{\alpha},\boldsymbol{\beta})\in\Pi_\lambda$. Thus, considering (14), any $(\boldsymbol{\alpha},\boldsymbol{\beta})\in\Pi_\lambda$ that satisfies $\gamma_{\mathrm{H}}(\boldsymbol{\lambda},\boldsymbol{\alpha}) = K\frac{\lambda_\nu}{\bar{p}_{\mathrm{d}\hat{\nu}}}$ is power-optimal. According to Corollary 2, when $\gamma_{\mathrm{H}}(\boldsymbol{\lambda},\boldsymbol{\alpha}) = K\frac{\lambda_\nu}{\bar{p}_{\mathrm{d}\hat{\nu}}}$, the only stabilizing $\boldsymbol{\beta}$ is $(1,1)$ and Q_ν is at stability edge. This completes the proof of power-optimal policies. Also, note that at a power-optimal policy, the energy consumption rate at node R is minimized since Q_ν is always backlogged at stability edge, and thus, all packets of $\mathrm{Q}_{\hat{\nu}}$ are transmitted in coded form. As a result, we have $\gamma_{\mathrm{C}} = K\frac{\lambda_\nu}{\bar{p}_{\mathrm{d}\hat{\nu}}}$. On the other hand, no energy is wasted (blocked) at node R since $\gamma_{\mathrm{H}} = \gamma_{\mathrm{C}}$ (see Lemma 2).

Let us define $\alpha'_i = \frac{1}{\alpha_i}$. Then, using (7) and $\gamma_{\mathrm{H}}(\boldsymbol{\lambda},\boldsymbol{\alpha}) = K\frac{\lambda_\nu}{\bar{p}_{\mathrm{d}\hat{\nu}}}$, α'_2 is written as $\alpha'_2 = g(\alpha'_1) = 1+\frac{\bar{p}_{\mathrm{u}2}}{\lambda_2\bar{e}_2}[K\frac{\lambda_\nu}{\bar{p}_{\mathrm{d}\nu}} - \frac{\lambda_1\bar{e}_1}{\bar{p}_{\mathrm{u}1}}(\alpha'_1-1)]$. Then, from $1\le\alpha'_2\le\frac{\bar{p}_{\mathrm{u}2}}{\lambda_2}$, we conclude that $g^{-1}(\frac{\bar{p}_{\mathrm{u}2}}{\lambda_2}) \le \alpha'_1 \le g^{-1}(1)$. On the other hand, $1\le\alpha'_1\le\frac{\bar{p}_{\mathrm{u}1}}{\lambda_1}$. Therefore, we have $\max\{g^{-1}(\frac{\bar{p}_{\mathrm{u}2}}{\lambda_2}),1\}\le\alpha'_1\le\min\{\frac{\bar{p}_{\mathrm{u}1}}{\lambda_1},g^{-1}(1)\}$. The right-hand side of this inequality is positive since $g^{-1}(1)>0$. Thus, we have $\frac{1}{\min\{\frac{\bar{p}_{\mathrm{u}1}}{\lambda_1},g^{-1}(1)\}}\le\alpha_1\le\frac{1}{\max\{g^{-1}(\frac{\bar{p}_{\mathrm{u}2}}{\lambda_2}),1\}}$. Also, when $\boldsymbol{\lambda}\in\partial\mathcal{R}$, the only power-optimal TS policy is $\boldsymbol{\alpha}^*_{\boldsymbol{\lambda}}$. In fact, it is the only stabilizing TS policy that satisfies $\gamma_{\mathrm{H}}(\boldsymbol{\lambda},\boldsymbol{\alpha}) = K\frac{\lambda_\nu}{\bar{p}_{\mathrm{d}\hat{\nu}}}$ (see Corollary 3). □

V. Average Delay Analysis of the Proposed TWRN

In this section, we derive the average delay of the proposed TWRN for a given TS-ONC policy. It is worth mentioning that in non-EH TWRNs, the delay-optimal ONC policy is $\boldsymbol{\beta} = (1,1)$. Using the analysis of average delay in this section, we show in Section VI that unlike the non-EH TWRNs, the delay-optimal NC policy in an EH TWRN may wait for a coding opportunity, i.e., $\beta_i<1$ ($i\in\{1,2\}$), when enough energy exists. According to the Little's law, the average delay at node R is written as

$$\tau_{\mathrm{avg}}(\boldsymbol{\alpha},\boldsymbol{\beta}) = \frac{\bar{q}_1+\bar{q}_2}{\lambda_1+\lambda_2}, \tag{16}$$

where $\tau_{\mathrm{avg}}(\boldsymbol{\alpha},\boldsymbol{\beta})$ is the average delay at node R under policy $(\boldsymbol{\alpha},\boldsymbol{\beta})$. Moreover, $\bar{q}_1$ and $\bar{q}_2$ are the average number of data packets at Q_1 and Q_2, respectively. Note that the difficulty in deriving τ_{avg} lies in modeling three inteacting queues, Q_1, Q_2, and Q_{e}. In the following, we propose two inter-related QBDs for deriving τ_{avg}.

This article has been accepted for publication in a future issue of this journal, but has not been fully edited. Content may change prior to final publication. Citation information: DOI 10.1109/TVT.2020.3031662, IEEE Transactions on Vehicular Technology

A. Proposed Inter-related QBDs

The system state is represented by $(q_1, q_2, q_{\rm e})$, where $q_i \in \mathbb{Z}^*$ $(i \in \{1,2\})$ and $q_{\rm e} \in \{0,1,...,N\}$ denote the number of data packets and energy units at $\rm Q_{\it i}$ and $\rm Q_e$, respectively, at the beginning of the downlink subslot. Thus, a slot is considered as a downlink subslot and two consecutive uplink subslots. The system state in our scenario evolves according to a Markov chain since all network parameters, e.g., channel detection probabilities and EH profiles, are independent and identically distributed across different subslots. However, the underlying Markov chain is very hard to solve since the first and second entries of the system state, i.e., q_1 and q_2, are not finite and the data queues and energy buffer are interacting. To tackle this problem, we follow an approach similar to [24]. In particular, by limiting the system state in the first and second dimensions, we approximate the system Markov chain with two inter-related Markov chains, denoted by $\rm MC_1$ and $\rm MC_2$, respectively. Then, $\rm MC_1$ and $\rm MC_2$ are solved iteratively in order to derive the average delay. In the following, we introduce $\rm MC_{\it i}$ $(i \in \{1,2\})$ in detail.

Let $j \neq i$, where $i, j \in \{1,2\}$. Then, the state of $\rm MC_{\it i}$ is represented as $(q_i, \tilde{q}_j, q_e)$, where $q_i \in \mathbb{Z}^*$ denotes the state of $\rm Q_{\it i}$, as in the original underlying Markov chain. Moreover, the state of $\rm Q_{\it j}$ is modeled by $\tilde{q}_j$, where $\tilde{q}_j \in \{0,1,...,m\}$, i.e., $\rm Q_{\it j}$ is approximated by m states instead of infinite ones. If $\tilde{q}_j \in \{0,1,...,m-1\}$, then there are exactly $\tilde{q}_j$ packets in $\rm Q_{\it j}$, i.e., $q_j = \tilde{q}_j$. However, when $\tilde{q}_j = m$, the number of data packets at $\rm Q_{\it j}$ is equal to or greater than m, i.e., $q_j \geq m$. Note that the number of states in $\rm MC_{\it i}$ is still infinite due to the first entry, q_i. However, we are able to solve $\rm MC_{\it i}$ since it is a QBD process [27]. According to the convention, each state in a QBD process is represented by an ordered-pair $(l, \overrightarrow{\phi})$, where the first and second entries, i.e., l and $\overrightarrow{\phi}$, denote the level and the phase of the QBD process, respectively. Therefore, if we denote by $\rm QBD_{\it i}$ as the QBD process corresponding to $\rm MC_{\it i}$, then, q_i and $\overrightarrow{\phi}_i = (\tilde{q}_j, q_e)$ represent the level and the phase of $\rm QBD_{\it i}$, respectively (see Fig. 4). We solve $\rm QBD_1$ and $\rm QBD_2$ iteratively to derive the $\tau_{\rm avg}$. In the following, we first derive the transition probabilities of the proposed QBDs and then, introduce an iterative algorithm for deriving $\tau_{\rm avg}$.

B. Transition probabilities

Let $X = (q_i, (\tilde{q}_j, q_{\rm e}))$ denote the current state of $\rm QBD_{\it i}$. Also, Z_i $(i \in \{1,2\})$ is equal to one if a packet is transmitted from $\rm Q_{\it i}$ and zero otherwise. Moreover, given the current state X, and the variables Z_i and Z_j, the conditional probabilities $F_i(q_i', a|X, Z_i)$ and $G_i(\tilde{q}_j', \tilde{a}|X, Z_j)$ associated to $\rm QBD_{\it i}$ are defined as the probabilities that the state of $\rm Q_{\it i}$ and $\rm Q_{\it j}$ become q_i' and $\tilde{q}_j'$ at the beginning of the next downlink subslot, respectively, while a and $\tilde{a}$ energy units are harvested from nodes $\rm S_{\it i}$ and $\rm S_{\it j}$ in the corresponding uplink subslots, respectively. Then, the transition probability from state X to state $Y = (q_i', (\tilde{q}_j', q_{\rm e}'))$ in $\rm QBD_{\it i}$, denoted by $Pr\{X \to Y\}$, is derived as ($q_{\rm e}' < N$, $L_1 = q_{\rm e}' - q_{\rm e} + K$, $L_2 = q_{\rm e}' - q_{\rm e}$)

$$Pr\{X \to Y\} = \begin{cases} \sum\limits_{a=0}^{L_1} F_i(q_i', a|X, Z_i = 1) G_i(\tilde{q}_j', L_1 - a|X, Z_j = 1); \\ \qquad\qquad q_i > 0,\ \tilde{q}_j > 0,\ q_{\rm e} \geq K, \\ \beta_i \sum\limits_{a=0}^{L_1} F_i(q_i', a|X, Z_i = 1) G_i(\tilde{q}_j', L_1 - a|X, Z_j = 0) + \\ (1-\beta_i) \sum\limits_{a=0}^{L_2} F_i(q_i', a|X, Z_i = 0) G_i(\tilde{q}_j', L_2 - a|X, Z_j = 0); \\ \qquad\qquad q_i > 0,\ \tilde{q}_j = 0,\ q_{\rm e} \geq K, \\ \beta_j \sum\limits_{a=0}^{L_1} F_i(q_i', a|X, Z_i = 0) G_i(\tilde{q}_j', L_1 - a|X, Z_j = 1) + \\ (1-\beta_j) \sum\limits_{a=0}^{L_2} F_i(q_i', a|X, Z_i = 0) G_i(\tilde{q}_j', L_2 - a|X, Z_j = 0); \\ \qquad\qquad q_i = 0,\ \tilde{q}_j > 0,\ q_{\rm e} \geq K, \\ \sum\limits_{a=0}^{L_2} F_i(q_i', a|X, Z_i = 0) G_i(\tilde{q}_j', L_2 - a|X, Z_j = 0); \text{otherwise.} \end{cases} \tag{17}$$

In the first case of (17), the packets of $\rm Q_1$ and $\rm Q_2$ are coded and transmitted with probability one, i.e., $Z_i = Z_j = 1$, since both queues are nonempty and enough energy exists. Consequently, K energy units are consumed and thus, in order to transit from $q_{\rm e}$ to $q_{\rm e}'$, $L_1 = q_{\rm e}' - q_{\rm e} + K$ energy units should be harvested. In this respect, the first factor in the summation indicates that a energy units out of $q_{\rm e}' - q_{\rm e} + K$ ones are harvested from $\rm S_{\it i}$ in the following uplink subslot i, while the rest are harvested from $\rm S_{\it j}$ in the following uplink subslot j. In the second case, a packet is transmitted from $\rm Q_{\it i}$ with probability β_i since $\rm Q_{\it i}$ is nonempty but $\rm Q_{\it j}$ is empty. The second additive term of this case states that if no transmission occurs (with probability $1-\beta_i$), we have $Z_i = Z_j = 0$ and $l_2 = q_{\rm e}' - q_{\rm e}$ energy units should be harvested in order to transit from $q_{\rm e}$ to $q_{\rm e}'$. Other cases are written in a similar way.

When $q_{\rm e}' = N$, the transition from $q_{\rm e}$ to $q_{\rm e}' = N$ happens if more than $N - q_{\rm e}$ ($N - q_{\rm e} + K$ in the case of transmission) energy units are harvested. In fact, the excess energy units will be blocked. Thus, when writing $Pr\{X \to Y\}$, the terms $\sum\limits_{a=0}^{L_2}(\sum\limits_{a=0}^{L_1}$ in the case of transmission) in (17) are replaced with $\sum\limits_{L_2=N-q_e}^{\infty}\sum\limits_{a=0}^{L_2}(\sum\limits_{L_1=N-q_e+K}^{\infty}\sum\limits_{a=0}^{L_1}$ in the case of transmission).

Now, we derive the conditional probabilities in (17). $F_i(q_i', a|X, Z_i = 1)$ is computed as

$$F_i(q_i', a|X, Z_i = 1) = \begin{cases} \bar{p}_{\rm d}{\it j}(1-\alpha_i) f_i(a) + \bar{p}_{\rm d}{\it j}\alpha_i(1-\bar{p}_{\rm u}{\it i}) 1(a=0); & q_i' = q_i - 1, \\ (1-\bar{p}_{\rm d}{\it j})(1-\alpha_i) f_i(a) + (1-\bar{p}_{\rm d}{\it j})\alpha_i(1-\bar{p}_{\rm u}{\it i}) 1(a=0) + \\ \bar{p}_{\rm d}{\it j}\alpha_i\bar{p}_{\rm u}{\it i} 1(a=0); & q_i' = q_i, \\ (1-\bar{p}_{\rm d}{\it j})\alpha_i\bar{p}_{\rm u}{\it i} 1(a=0); & q_i' = q_i + 1, \\ 0\ ; & \text{otherwise.} \end{cases} \tag{18}$$

where $f_i(a)$ is the probability that a energy units are harvested from a packet transmitted by node $\rm S_{\it i}$. The first term in the first case of (18) states that q_i decreases by one if the HoL packet in $\rm Q_{\it i}$ is transmitted successfully (with probability $\bar{p}_{\rm d}{\it j}$),

This article has been accepted for publication in a future issue of this journal, but has not been fully edited. Content may change prior to final publication. Citation information: DOI 10.1109/TVT.2020.3031662, IEEE Transactions on Vehicular Technology

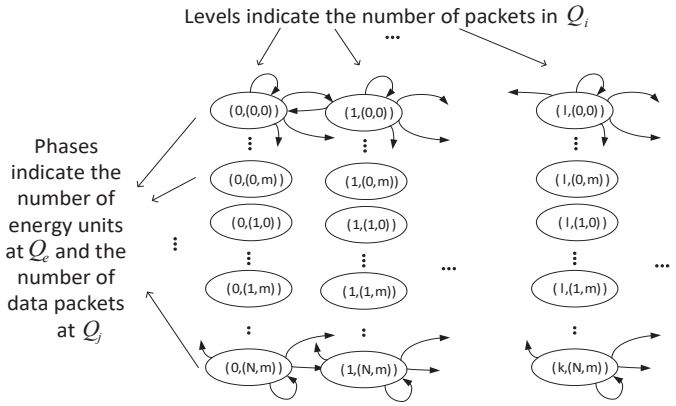

Fig. 4. QBD model.

node R selects the EH mode in subslot i (with probability $1-\alpha_i$), and a energy units are harvested from S_i (with probability $f_i(a)$). Moreover, according to the second term of the first case, if $a=0$, the transition also happens to q_i-1, when in the sequence of the aforementioned events, node R selects the DD mode instead of the EH one in subslot i (with probability α_i), however, it cannot detect the packet of node S_i successfully (with probability $1-\bar{p}_{\mathrm{u}i}$). The other cases are obtained similarly. Moreover, $F_i(q_i', a|X, Z_i=0)$ is derived from (18) by replacing $\bar{p}_{\mathrm{d}j}$ with zero since when $Z_i=0$, no packet is transmitted from Q_i in the downlink subslot. Next, we derive $G_i(\tilde{q}_j', a|X, Z_j=1)$ as follows.

For $0<\tilde{q}_j<m$:

$$G_i(\tilde{q}_j', \tilde{a}|X, Z_j=1)=$$
$$\begin{cases} \bar{p}_{\mathrm{d}i}(1-\alpha_j)f_j(\tilde{a})+\bar{p}_{\mathrm{d}i}\alpha_j(1-\bar{p}_{\mathrm{u}j})1(\tilde{a}=0); & \tilde{q}_j'=\tilde{q}_j-1,\\ (1-\bar{p}_{\mathrm{d}i})(1-\alpha_j)f_j(\tilde{a})+(1-\bar{p}_{\mathrm{d}i})\alpha_j(1-\bar{p}_{\mathrm{u}j})1(\tilde{a}=0)+ & \\ \bar{p}_{\mathrm{d}i}\alpha_j\bar{p}_{\mathrm{u}j}1(\tilde{a}=0); & \tilde{q}_j'=\tilde{q}_j,\\ (1-\bar{p}_{\mathrm{d}i})\alpha_j\bar{p}_{\mathrm{u}j}1(\tilde{a}=0); & \tilde{q}_j'=\tilde{q}_j+1,\\ 0\ ; & \text{otherwise.}\end{cases} \tag{19}$$

Note that since $\tilde{q}_j<m$ in (19), it represents the real number of data packets at Q_j. Moreover, for any choice of $0<\tilde{q}_j<m$, the transition can occur to the states $\tilde{q}_j$ and $\tilde{q}_j\pm1$. Thus, the transition probabilities in (19) are written exactly as in (18). However, when $\tilde{q}_j$ is equal to m, the transition to $\tilde{q}_j'=m-1$ or $\tilde{q}_j'=m$ is only possible. In this regard, when $\tilde{q}_j=m$, we have

$$G_i(\tilde{q}_j', \tilde{a}|X, Z_j=1)=$$
$$\begin{cases} \pi_{jm}\bar{p}_{\mathrm{d}i}(1-\alpha_j)f_j(\tilde{a})+\pi_{jm}\bar{p}_{\mathrm{d}i}\alpha_j(1-\bar{p}_{\mathrm{u}j})1(\tilde{a}=0); & \\ & \tilde{q}_j'=\tilde{q}_j-1,\\ (1-\pi_{jm}+\pi_{jm}(1-\bar{p}_{\mathrm{d}i}))\left((1-\alpha_j)f_j(\tilde{a})+\alpha_j1(\tilde{a}=0)\right)+ & \\ \pi_{jm}\bar{p}_{\mathrm{d}i}\alpha_j\bar{p}_{\mathrm{u}j}1(\tilde{a}=0); & \tilde{q}_j'=\tilde{q}_j,\\ 0\ ; & \text{otherwise.}\end{cases} \tag{20}$$

where π_{jm} is the probability that $q_j=m$, given that $\tilde{q}_j=m$ or equivalently, $q_j\geq m$. According to the first term in the first case of (20), the transition to $\tilde{q}_j-1$ occurs when q_j is exactly equal to m, a packet is transmitted successfully from Q_j in the downlink subslot, node R selects the EH mode in the following uplink subslot j, and it harvests $\tilde{a}$ energy units from the transmission of node S_j. According to the second term, in the case that $\tilde{a}=0$, the transition to $\tilde{q}_j-1$ also happens if in the sequence of the aforementioned events, node R selects the DD mode instead of the EH one in the following uplink subslot j, but does not detect the packet of node S_j successfully. The other cases are obtained in a similar way. Finally, for deriving $G_i(\tilde{q}_j', \tilde{a}|X, Z_j=0)$ in the cases $0\leq\tilde{q}_j<m$ and $\tilde{q}_j=m$, it is enough to replace $\bar{p}_{\mathrm{d}j}$ in (19) and (20) with zero, respectively, since when $Z_j=0$, no packet is transmitted from Q_j.

C. Deriving average delay

As can be seen from (17)-(20), the parameters of the transition probabilities of QBD_i ($i\in\{1,2\}$) are all known except π_{jm}. In fact, this parameter is related to the distribution of the number of data packets at Q_j and thus, can be derived from QBD_j since in QBD_j, we model the states of Q_j completely. Therefore, we solve QBD_1 and QBD_2 iteratively to derive the values of π_{1m} and π_{2m}. In particular, we first set some initial values for π_{1m} and π_{2m}. Then, in iteration t ($t\geq1$), first, the transition probabilities of QBD_i ($i=2-\mathrm{mod}(t,2)$), are updated using π_{jm}. Then, QBD_i is solved, i.e., the stationary probability of different states are derived, using the related algorithms in [27]. Consequently, by solving QBD_i, π_{im} is updated. The iterations are repeated until a certain convergence criterion is met. Moreover, in each iteration, after QBD_i is solved ($i\in\{1,2\}$), π_{im} is updated as follows

$$\pi_{im}=\frac{\boldsymbol{\pi}_{i0}(\mathbf{R}_i)^m\mathbf{1}}{\sum_{l=m}^{\infty}\boldsymbol{\pi}_{i0}(\mathbf{R}_i)^l\mathbf{1}}, \tag{21}$$

where $\boldsymbol{\pi}_{i0}$ is the steady state probability vector of the states $(0,(\tilde{q}_j,q_e))$ at QBD_i, where $\tilde{q}_j\in\{0,1,...,m\}$ and $q_e\in\{0,1,...,N\}$. Also, $\mathbf{1}$ is the all-one column vector. Moreover, $\mathbf{R}_i$[2] is a matrix related to QBD_i and is derived according to some algorithms in [27]. In (21), $\boldsymbol{\pi}_{i0}(\mathbf{R}_i)^l$ is the probability vector of the states in level l, i.e., the states with $q_i=l$ [27]. Once the aforementioned iterative algorithm for solving QBDs is converged, the average queue length $\bar{q}_i$ ($i\in\{1,2\}$) is derived as

$$\overline{q_i}=\sum_{q_i=0}^{\infty}q_i\boldsymbol{\pi}_{i0}(\mathbf{R}_i)^{q_i}\mathbf{1}=\boldsymbol{\pi}_{i0}\mathbf{R}_i(\mathbf{I}-\mathbf{R}_i)^{-2}\mathbf{1}. \tag{22}$$

VI. Numerical Results

In this section, we present our numerical results to evaluate the effect of different system parameters on the stability region as well as optimal throughput of the network, and power-optimal and delay-optimal policies corresponding to some arbitrary point in the stability region, i.e., at some specific satisfying rates. The simulation has been done in MATLAB environment and the results are reported in some figures to validate the analytical approach. In the following, we first consider a practical system setup and derive the parameters of our system model, including the average detection probabilities $\bar{p}_{\mathrm{d}i}$, $\bar{p}_{\mathrm{u}i}$, and EH profile $f_i(.)$ ($i\in\{1,2\}$). Then, the numerical results are presented.

[2]The dimension of $\mathbf{R}_i$ is $m(N+1)\times m(N+1)$ and the entry (k,k') is the expected number of visits to the state $(n+1,k')$, before a return to level n or previous levels given that the process starts from state (n,k).

This article has been accepted for publication in a future issue of this journal, but has not been fully edited. Content may change prior to final publication. Citation information: DOI 10.1109/TVT.2020.3031662, IEEE Transactions on Vehicular Technology

TABLE II
TYPICAL VALUES OF SYSTEM PARAMETERS

Parameter	Value	Parameter	Value
$P_{\mathrm{S}_1} = P_{\mathrm{S}_2}$	30 dBm	P_{R}	-27dBm
All channel gains	1	σ^2	-97 dBm
$d_{\mathrm{S}_1\mathrm{R}} = d_{\mathrm{S}_2\mathrm{R}}$	15 m	$G_{\mathrm{S}} = G_{\mathrm{R}}$	8 dBi
λ	0.33 m	C	0.1
d_0	1 m	ϵ	10^{-7} J
κ	0.6	N	100

A. Simulation Setup

We consider Nakagami block fading channels with shape parameter $M = 2$ and derive the average detection probabilities, $\bar{p}_{\mathrm{u}i}$ and $\bar{p}_{\mathrm{d}i}$, through simulating the corresponding wireless channels. Specifically, by assuming BPSK modulation and uncoded transmissions at the wireless nodes, we calculate the detection probability of a packet as $(1 - Q(\sqrt{2w_{\mathrm{XY}}}))^L$, where L is the packet length, w_{XY} is the signal-to-noise ratio at the receiver of X to Y transmission, and $Q(.)$ is the Q-function. Moreover, $w_{\mathrm{XY}} = C\Lambda\frac{P_{\mathrm{X}}\mathrm{E}(|h_{\mathrm{XY}}|^2)}{\sigma^2 d_{\mathrm{XY}}^{\eta}}$ [25], where P_{X} is the transmission power of node X, h_{XY} is the gain of the channel X-Y, σ^2 is the noise power, d_{XY} is the distance between the nodes X and Y, η is the path loss exponent, $\mathrm{E}(.)$ is the mean operator, C models the shadow fading effect, and Λ is a constant related to the path loss model. In particular, $\Lambda = \frac{G_{\mathrm{S}}G_{\mathrm{R}}\lambda^2 d_0^{\eta-2}}{4\pi^2}$, where G_{X} is the antenna gain at node X, λ is the carrier wavelength, and d_0 is the close-in reference model. Typical values of the parameters are listed in Table II, using [25]. Using Table II, we have $\Lambda = 0.027$, $\bar{p}_{\mathrm{u}1} = \bar{p}_{\mathrm{u}2} \approx 1$, and $\bar{p}_{\mathrm{d}1} = \bar{p}_{\mathrm{d}2} = 0.23$.

Moreover, let Γ_i be the continuous random variable denoting the harvested energy in subslot i. Then, $\Gamma_i = \kappa C\Lambda\frac{P_{\mathrm{S}_i}|h_{\mathrm{S}_i\mathrm{R}}|^2}{d_{\mathrm{S}_i\mathrm{R}}^{\eta}}$, where κ is the EH conversion efficiency. Moreover, Γ_i has the same distribution as $|h_{\mathrm{S}_i\mathrm{R}}|^2$, which is Gamma. We discretize Γ_i to derive $f_i(.)$ $(i \in \{1, 2\})$, i.e., the probability of harvesting m energy units in subslot i $(i \in \{1, 2\})$. As such, considering each energy unit to be ϵ Joules, $f_i(m)$ is derived as $f_i(m) = \Pr((m - 0.5)\epsilon \le \Gamma_i \le (m + 0.5)\epsilon)$ [26]. Then, using Table II and choosing each time slot as the time unit,we have $\bar{e}_1 = \bar{e}_2 = 1.6$ energy units. Moreover, $K = \frac{P_{\mathrm{R}}}{\epsilon} = 20$ energy units. Also, regrading the size of energy buffer, i.e., $N = 100$, the assumption $N \ge 2K$ holds. On the other hand, it is observed that $F(m) \ge 1 - 0.001$ for $m \ge 10$ and thus, $a^{\max} = 10$ (see Section II-D). Therefore, the assumption $a^{\max} \le K$ holds. Note that in our simulations, we do not truncate the EH profiles and apply the real ones.

B. Simulation and Analytical Results

In Fig. 5, the stability region of the network is depicted for different values of K. For deriving the border of stability region by simulation, we first choose an arbitrary λ_1. Then, using Corollary 3, we increase λ_2 until Q_ν becomes unstable under the policy $(\boldsymbol{\alpha}^*_{\boldsymbol{\lambda}}, (1, 1))$. It can be seen that the simulation results are almost matched with the analytical ones. Note that increasing K, has a two-fold effect on the optimal throughput. On the one hand, it may increase the optimal throughput due to increasing detection probabilities in downlink channels. On the other hand, it may decrease the optimal throughput since the packets have to wait longer to accumulate enough energy for transmission. When K is increased from 15 to 30 in Fig. 5, the former effect dominates the latter one, leading to the expansion of the stability region. However, when K is increased to 40, the detection probabilities do not change considerably and thus, the latter effect dominates the former one, resulting in the shrink of the stability region.

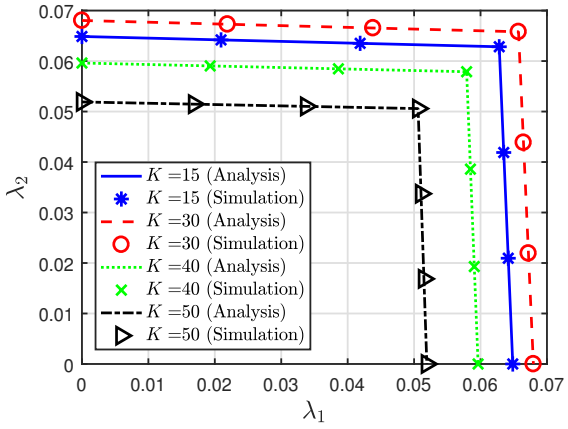

Fig. 5. Stability region of the network.

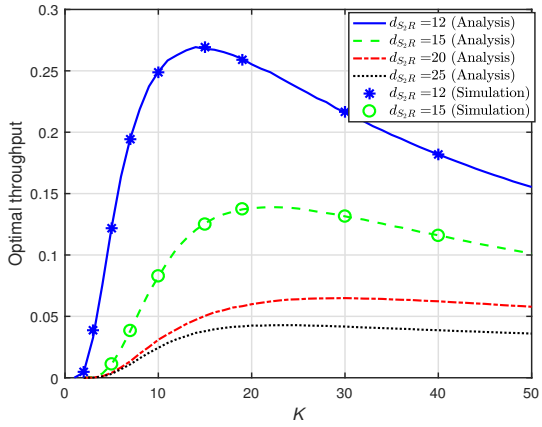

Fig. 6. Optimal throughput versus the detection probability of channel R-S_2.

In Fig. 6, the optimal throughput, derived in (13), is plotted versus K, at different values of d_{S_2R}. It is worth noting that the EH profile, $f(.)$, changes with d_{S_2R}, so does $a^{\max}$, e.g., $a^{\max}$ is 19 and 10 at $d_{\mathrm{S}_2R} = 12$ and 15, respectively. Then, at each value of d_{S_2R}, the analytical results are valid for $K \ge a^{\max}$. Moreover, to check the accuracy of our results when $K \le a^{\max}$, we have added some simulation results to Fig. 6, in the cases of $d_{\mathrm{S}_2R} = 12, 15$. As can be seen, even when $K \le a^{\max}$, the simulation results match with the analytical ones well enough. In fact the assumption $K \ge a^{\max}$ helped us to prove that p_{b} is zero when Q_ν is always backlogged (see Lemma 2), which is the case in throughput-optimal policy. Here, although the assumption does not hold, but p_{b} is very small under the condition of Lemma 2, leading to our analytical results still being accurate. According to our simulation results, p_{b} only becomes considerable when the value of K results in very poor downlink channels (e.g.,

This article has been accepted for publication in a future issue of this journal, but has not been fully edited. Content may change prior to final publication. Citation information: DOI 10.1109/TVT.2020.3031662, IEEE Transactions on Vehicular Technology

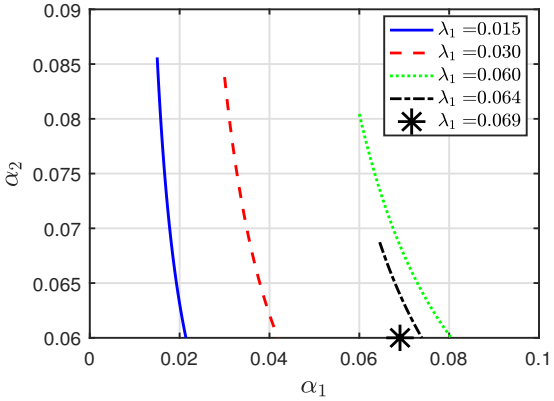

Fig. 7. Power optimal TS policies at $\lambda_2 = 0.06$.

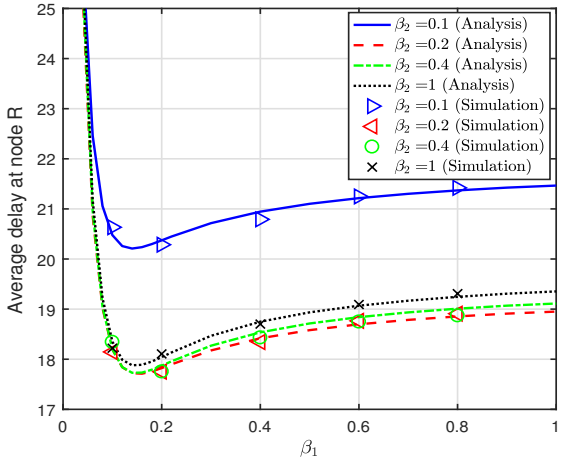

Fig. 8. Average delay at node R versus NC probabilities ($\boldsymbol{\lambda} = (0.06, 0.09)$, $d_{\mathrm{S_1R}} = 12$, $d_{\mathrm{S_2R}} = 12$).

$K \leq 2$ in Fig. 6). Here, the energy arrival rate at $\mathrm{Q_e}$ is high since DD probabilities are set very small to store less data, while only a small energy is departed in each transmission (K), leading to a large p_{b}. Also, as can be seen in Fig. 6, at a fixed $d_{\mathrm{S_2}R}$, there is an optimum value for K due to the aforementioned contradicting effects of K on the throughput.

In Fig. 7, the TS policy, i.e., (α_1, α_2), of the power-optimal policy, derived in Proposition 3, is plotted at $\lambda_2 = 0.06$ and different values of λ_1, where $(\lambda_1, \lambda_2) \in \mathcal{R}$. In these cases, for $\lambda_1 \leq 0.06$, we have $\mathrm{Q}_\nu = \mathrm{Q}_2$, and for $\lambda_1 > 0.06$, $\mathrm{Q}_\nu = \mathrm{Q}_1$. As can be seen in Fig. 7, at a fixed α_2, the power-optimal α_1 increases with λ_1 as long as $\lambda_1 \leq 0.06$. This is due to the fact that for $\lambda_1 \leq 0.06$, Q_2 is at stability edge and thus, the packets of Q_1 are transmitted with packets of Q_2 in coded form and do not consume energy separately. Therefore, although λ_1 increases, there is no need to harvest more energy. In this regard, the EH rate from node S_1, i.e., $\frac{1-\alpha_1}{\bar{p}_{\mathrm{u}1}\alpha_1}\lambda_1\bar{e}_1$, should remain constant, which happens by increasing α_1. However, when $\lambda_1 > 0.06$, α_1 decreases with λ_1 at a fixed α_2. Here, Q_1 is at stability edge and thus, all energy units are consumed by the packets of Q_1. Therefore, if λ_1 increases, more energy is needed to keep Q_1 stable. Hence, α_1 decreases to increase the EH rate from node S_1. As can be seen in Fig. 7, when λ_1 increases, the ranges of power-optimal α_1 and α_2 shrink. This is due to the fact that the data queues become more crowded and the power-optimal policy should harvest more energy to keep the data queues stable and thus, is not free to change α_1 and α_2 in a large interval. Moreover, at $\lambda = 0.069$, which is on the border of the stability region, there is only one power-optimal policy, i.e., $\boldsymbol{\alpha} = \boldsymbol{\alpha}^*_{\boldsymbol{\lambda}}$. In fact, $\boldsymbol{\alpha}^*_{\boldsymbol{\lambda}}$ is the only stabilizing TS policy when $\boldsymbol{\lambda} \in \partial\mathcal{R}$, according to Corollary 3.

In Fig. 8, the average delay at node R is plotted versus β_1 and different values of β_2, given that $\boldsymbol{\lambda} = (0.06, 0.09)$. Also, we set $\boldsymbol{\alpha} = \boldsymbol{\alpha}^*_{\boldsymbol{\lambda}}$ since in this case, the EH rate is maximized. As observed in Fig. 8, when β_1 increases from zero, the average delay decreases at first since by increasing β_1 the packets at Q_1 are transmitted faster, in uncoded form. However, when β_1 becomes large enough, the uncoded transmissions at Q_1 leads to a larger energy consumption rate and thus, more frequent depletion of the energy buffer. Thus, the average delay increases. From Fig. 8, it can be seen that, unlike the case of non-EH TWRNs, the delay-optimal value of $\boldsymbol{\beta}$ is not equal to $(1, 1)$. If $\boldsymbol{\beta}$ is chosen to be $(1, 1)$, the average delay increases about 9% compared to the optimal average delay, happening approximately at $\boldsymbol{\beta} = (0.16, 0.2)$.

VII. Conclusion

We considered a TWRN with a WEH relay that applies an ONC policy for transmission of the packets, either in coded or uncoded form, and a TS policy to receive data and energy from transmissions of two sources. We derived the stability region of the proposed network by deriving stabilizing TS and ONC policies at the relay. We concluded that waiting in ONC does not contribute to the stability region. Moreover, we derived the throughput-optimal and power-optimal policies. It was shown that in the these policies, the ONC parameter related to the queue with maximum total arrival rate is equal to one. Then, to derive the average delay of the packets at the relay, we modeled the system with two inter-related QBDs. The proposed QBDs modeled the states of the data queues and energy buffer. We showed that unlike the non-EH TWRNs, the delay-optimal policy in an EH-TWRN may decide to wait for a coding opportunity. Finally, we validated our analytical approach with several numerical results.

Appendix

A. Proof of Lemma 1

Part (a): We prove the lemma by contradiction. If node R is unstable, then, according to Definition 2, at least one of the queues is unstable. Assume that Q_ν is stable and $\mathrm{Q}_{\hat{\nu}}$ is unstable. Then, according to Remark 1, we have $\lambda_{\mathrm{o}\nu} = \frac{\lambda_\nu}{\bar{p}_{\mathrm{d}\hat{\nu}}}$ at Q_ν , while $\lambda_{\mathrm{o}\hat{\nu}} < \frac{\lambda_{\hat{\nu}}}{\bar{p}_{\mathrm{d}\hat{\nu}}}$ at $\mathrm{Q}_{\hat{\nu}}$. Therefore, using $\frac{\lambda_{\hat{\nu}}}{\bar{p}_{\mathrm{d}\nu}} \leq \frac{\lambda_\nu}{\bar{p}_{\mathrm{d}\hat{\nu}}}$, we conclude that $\lambda_{\mathrm{o}\nu} > \lambda_{\mathrm{o}\hat{\nu}}$. On the other hand, $\mathrm{Q}_{\hat{\nu}}$ is always backlogged due to instability, according to Remark 2. Thus, all packets of Q_ν are coded and transmitted with the packets of $\mathrm{Q}_{\hat{\nu}}$, implying that the total departure rate at Q_ν is less than or equal to the total departure rate at $\mathrm{Q}_{\hat{\nu}}$, i.e., $\lambda_{\mathrm{o}\nu} \leq \lambda_{\mathrm{o}\hat{\nu}}$. This contradicts with the previous result, $\lambda_{\mathrm{o}\nu} > \lambda_{\mathrm{o}\hat{\nu}}$. When Q_ν is unstable, it is always backlogged, according to Remark 2. Then, every packet at $\mathrm{Q}_{\hat{\nu}}$ is coded and transmitted with a packet at Q_ν, implying that $\lambda_{\mathrm{c}} = \lambda_{\mathrm{o}\hat{\nu}}$. Thus, $\gamma_{\mathrm{C}} = K\lambda_{\mathrm{o}\nu}$, according to (9).

Part (b): We prove the second part of the lemma by contradiction, i.e., we assume that only $\mathrm{Q}_{\hat{\nu}}$ is at stability edge. Then, unlike Q_{ν}, $\mathrm{Q}_{\hat{\nu}}$ is always backlogged, according to Remark 2. This implies that all packets at Q_{ν} are transmitted in coded form, with a rate less than the total departure rate at $\mathrm{Q}_{\hat{\nu}}$, i.e., we have $\lambda_{\mathrm{o}\nu} < \lambda_{\mathrm{o}\hat{\nu}}$. On the other hand, due to the stability of node R, both queues are stable, and thus, we have $\lambda_{\mathrm{o}\hat{\nu}} = \frac{\lambda_{\hat{\nu}}}{\bar{p}_{\mathrm{d}\hat{\nu}}}$ and $\lambda_{\mathrm{o}\nu} = \frac{\lambda_{\nu}}{\bar{p}_{\mathrm{d}\hat{\nu}}}$, according to Remark 1. Therefore, we conclude that $\frac{\lambda_{\nu}}{\bar{p}_{\mathrm{d}\hat{\nu}}} < \frac{\lambda_{\hat{\nu}}}{\bar{p}_{\mathrm{d}\nu}}$, which contradicts with (5). When Q_{ν} is at stability edge, it is always backlogged, according to Remark 2. Thus, similar to Part (a), we have $\gamma_{\mathrm{C}} = K\lambda_{\mathrm{o}\nu}$. On the other hand, since Q_{ν} is stable at stability edge, we have $\lambda_{\mathrm{o}\nu} = \frac{\lambda_{\nu}}{\bar{p}_{\mathrm{d}\hat{\nu}}}$, using Remark 1. Therefore, $\gamma_{\mathrm{C}} = K\frac{\lambda_{\nu}}{\bar{p}_{\mathrm{d}\hat{\nu}}}$.

B. Proof of Lemma 2

We first show that if Q_{ν} is always backlogged and $\beta_{\nu} = 1$, then $p_b = 0$. Let q_e and q'_e denote the number of energy units at the beginning and ending of a typical downlink subslot. In the case of $K \leq q_e \leq N$, a packet is transmitted from Q_{ν} since enough energy exists, Q_{ν} is backlogged, and $\beta_{\nu} = 1$. Consequently, we have $q'_e \leq N - K$ since K energy units are consumed. On the other hand, in the case if $q_e < K$, no transmission happens, leading to $q'_e = q_e$. The equations $q_e < K$ and $q'_e = q_e$, along with the assumption $N \geq 2K$ introduced in Section II-D, results in $q'_e < K \leq N - K$. Thus, in either cases, we have $q'_e \leq N - K$. Therefore, no blocking happens in the uplink subslots of the next slot since due to our assumption $a^{\max} \leq K$ (see Section II-D), the number of energy units harvested in a slot is less than or equal to K. For proving the "only if" part, note that when Q_{ν} is backlogged and $\beta_{\nu} < 1$, despite the presence of data packets at Q_{ν}, the transmission may not occur when $K \leq q_{\mathrm{e}} \leq N$. In this case, it is probable that the energy units are blocked if $q_{\mathrm{e}} > N - K$.

C. Proof of Lemma 3

Part (a): Assume that $(\boldsymbol{\alpha}, \boldsymbol{\beta}) \in \Pi_{\boldsymbol{\lambda}}$. Then, node R and consequently, Q_{ν}, are stable under the policy $(\boldsymbol{\alpha}, \boldsymbol{\beta})$, i.e., we have $\frac{\lambda_{\nu}}{\bar{p}_{\mathrm{d}\hat{\nu}}} = \lambda_{\mathrm{o}\nu}$, according to Remark 1. Thus, $K\frac{\lambda_{\nu}}{\bar{p}_{\mathrm{d}\hat{\nu}}} = K\lambda_{\mathrm{o}\nu}$. Note that $K\lambda_{\mathrm{o}\nu}$ is the energy consumption rate at Q_{ν} due to the packet transmission, which is definitely less than or equal to the EH rate, i.e., $\gamma_{\mathrm{H}}(\boldsymbol{\lambda}, \boldsymbol{\alpha})$. Thus, we have $K\frac{\lambda_{\nu}}{\bar{p}_{\mathrm{d}\hat{\nu}}} \leq \gamma_{\mathrm{H}}(\boldsymbol{\lambda}, \boldsymbol{\alpha})$.

Part (b): We prove this part by contradiction. Assume that $\gamma_{\mathrm{H}}(\boldsymbol{\lambda}, \boldsymbol{\alpha}) \geq K\frac{\lambda_{\nu}}{\bar{p}_{\mathrm{d}\hat{\nu}}}$ and $\boldsymbol{\beta} \in \mathcal{B}_{\boldsymbol{\lambda}}$ but $(\boldsymbol{\alpha}, \boldsymbol{\beta}) \notin \Pi_{\boldsymbol{\lambda}}$, i.e., node R is unstable under the policy $(\boldsymbol{\alpha}, \boldsymbol{\beta})$. Consequently, Q_{ν} is unstable, according to Lemma 1(a). This results in $K\frac{\lambda_{\nu}}{\bar{p}_{\mathrm{d}\hat{\nu}}} > K\lambda_{\mathrm{o}\nu}$, according to Remark 1, and $\gamma_{\mathrm{C}} = K\lambda_{\mathrm{o}\nu}$, according to Lemma 1. On the other hand, since Q_{ν} is always backlogged when unstable and $\beta_{\nu} = 1$, we have $\gamma_{\mathrm{C}} = \gamma_{\mathrm{H}}$, according to Lemma 2. Hence, from $K\frac{\lambda_{\nu}}{\bar{p}_{\mathrm{d}\hat{\nu}}} > K\lambda_{\mathrm{o}\nu}$, $\gamma_{\mathrm{C}} = K\lambda_{\mathrm{o}\nu}$, and $\gamma_{\mathrm{C}} = \gamma_{\mathrm{H}}$, we conclude $\gamma_{\mathrm{H}} < K\frac{\lambda_{\nu}}{\bar{p}_{\mathrm{d}\hat{\nu}}}$, which is a contradiction.

D. Proof of Lemma 4: parts (a) and (b)

The "if" part of Lemma 4(a) is concluded from Lemma 3(b), i.e., if $\gamma_{\mathrm{H}}(\boldsymbol{\lambda}, \boldsymbol{\alpha}) = K\frac{\lambda_{\nu}}{\bar{p}_{\mathrm{d}\hat{\nu}}}$ and $\boldsymbol{\beta} \in \mathcal{B}_{\boldsymbol{\lambda}}$, then $(\boldsymbol{\alpha}, \boldsymbol{\beta}) \in \Pi_{\boldsymbol{\lambda}}$. To prove the "only if" part, we first show that if $\gamma_{\mathrm{H}}(\boldsymbol{\lambda}, \boldsymbol{\alpha}) = K\frac{\lambda_{\nu}}{\bar{p}_{\mathrm{d}\hat{\nu}}}$ and $(\boldsymbol{\alpha}, \boldsymbol{\beta}) \in \Pi_{\boldsymbol{\lambda}}$, then Q_{ν} is at stability edge. On the one hand, $(\boldsymbol{\alpha}, \boldsymbol{\beta}) \in \Pi_{\boldsymbol{\lambda}}$ implies that Q_{ν} is stable under $(\boldsymbol{\alpha}, \boldsymbol{\beta})$, i.e., $\frac{\lambda_{\nu}}{\bar{p}_{\mathrm{d}\hat{\nu}}} \leq \mu_{\nu}$, according to Remark 1. On the other hand, μ_{ν} cannot be greater than $\frac{\gamma_{\mathrm{H}}(\boldsymbol{\lambda}, \boldsymbol{\alpha})}{K}$, i.e., $\mu_{\nu} \leq \frac{\gamma_{\mathrm{H}}(\boldsymbol{\lambda}, \boldsymbol{\alpha})}{K}$. Therefore, by $\gamma_{\mathrm{H}}(\boldsymbol{\lambda}, \boldsymbol{\alpha}) = K\frac{\lambda_{\nu}}{\bar{p}_{\mathrm{d}\hat{\nu}}}$, we have $\mu_{\nu} = \frac{\lambda_{\nu}}{\bar{p}_{\mathrm{d}\hat{\nu}}}$, i.e., Q_{ν} is at stability edge, according to Remark 1. Hence, $\gamma_{\mathrm{C}} = K\frac{\lambda_{\nu}}{\bar{p}_{\mathrm{d}\hat{\nu}}}$, according to Lemma 1(b), and thus, $\gamma_{\mathrm{C}} = \gamma_{\mathrm{H}}$. When Q_{ν} is at stability edge and thus, always backlogged, $\gamma_{\mathrm{C}} = \gamma_{\mathrm{H}}$ is achieved only if $\boldsymbol{\beta} \in \mathcal{B}_{\boldsymbol{\lambda}}$, according to Lemma 2.

REFERENCES

[1] W. Guo, S. Zhou, Y. Chen, S. Wang, X. Chu, and Z. Niu, "Simultaneous Information and Energy Flow for IoT Relay Systems with Crowd Harvesting," in *IEEE Commun. Mag.*, vol. 54, no. 11, pp. 143-149, Nov. 2016.

[2] K. Huang and E. Larsson, "Simultaneous Information and Power Transfer for Broadband Wireless Systems," *IEEE Trans. Signal Process.*, vol. 61, no. 23, pp. 59275941, Dec. 2013.

[3] C. Zhong, H. A. Suraweera, G. Zheng, I. Krikidis, and Z. Zhang, "Wireless Information and Power Transfer With Full Duplex Relaying," *IEEE Trans. Commun.*, vol. 62, no. 10, pp. 3447-3461, Oct. 2014.

[4] K. Xiong, P. Fan, C. Zhang, and K. B. Letaief, "Wireless Information and Energy Transfer for Two-Hop Non-Regenerative MIMO-OFDM Relay Networks," *IEEE J. Sel. Areas Commun.*, vol. 33, no. 8, pp. 1595-1611, Aug. 2015.

[5] M. Mohammadi, B. K. Chalise, H. A. Suraweera, C. Zhong, G. Zheng, and I. Krikidis, "Throughput Analysis and Optimization of Wireless-Powered Multiple Antenna Full-Duplex Relay Systems," *IEEE Trans. Commun.*, vol. 64, no. 4, pp. 1769-1785, April 2016.

[6] M. Xiao and M. Skoglund, "Multiple-user Cooperative Communications Based on Linear Network Coding, *IEEE Trans. Commun.*, vol. 58, no. 12, pp. 3345-3351, Dec. 2010.

[7] P. Popovski and H. Yomo, "Physical Network Coding in Two-Way Wireless Relay Channels," *IEEE International Conference on Communications*, Glasgow, 2007, pp. 707-712.

[8] R. H. Y. Louie, Y. Li, and B. Vucetic, "Practical physical layer network coding for two-way relay channels: performance analysis and comparison," *IEEE Trans. Wireless Commun.*, vol. 9, no. 2, pp. 764-777, Feb. 2010.

[9] M. H. Amerimehr and F. Ashtiani, "Delay and Throughput Analysis of a Two-Way Opportunistic Network Coding-Based Relay Network," *IEEE Trans. Wireless Commun.*, vol. 13, no. 5, pp. 2863-2873, May 2014.

[10] C. Peng, F. Li, and H. Liu, "Optimal Power Splitting in Two-Way Decode-and-Forward Relay Networks," *IEEE Commun. Letters*, vol. 21, no. 9, pp. 2009-2012, Sept. 2017.

[11] L. Shi, Y. Ye, R. Q. Hu, and H. Zhang, "System Outage Performance for Three-Step Two-Way Energy Harvesting DF Relaying," *IEEE Trans. on Vehicular Tech.*, 2019.

[12] S. Modem and S. Prakriya, "Performance of Analog Network Coding Based Two-Way EH Relay With Beamforming," *IEEE Trans. on Commun.*, vol. 65, no. 4, pp. 1518-1535, April 2017.

[13] T. P. Do, I. Song, and Y. H. Kim, "Simultaneous Wireless Transfer of Power and Information in a Decode-and-Forward Two-Way Relaying Network," *IEEE Trans. on Wireless Commun.*, vol. 16, no. 3, pp. 1579-1592, March 2017.

[14] H. Cao, L. Fu, and H. Dai, "Throughput analysis of the two-way relay system with network coding and energy harvesting," *IEEE International Conference on Communications (ICC)*, Paris, France, 2017, pp. 1-6.

[15] Z. Zhang, Y. Lu, Y. Huang, and P. Zhang, "Neural Network-based Relay Selection in Two-way SWIPT-enabled Cognitive Radio Networks," *IEEE Trans. on Vehicular Tech.*, 2020.

[16] Q. Li and L. Yang, "Robust Optimization for Energy Efficiency in MIMO Two-Way Relay Networks With SWIPT," *IEEE Systems Journal*, vol. 14, no. 1, pp. 196-207, March 2020.

[17] N. Gautam and A. Mohapatra, "Efficiently Operating Wireless Nodes Powered by Renewable Energy Sources" *IEEE J. Sel. Areas Commun.*, vol. 33, no. 8, pp. 1706-1716, Aug. 2015.

[18] Z. Chen, Y. Dong, P. Fan, and K. Ben Letaief, "Optimal Throughput for Two-Way Relaying: Energy Harvesting and Energy Co-Operation," *IEEE J. Sel. Areas Commun.*, vol. 34, no. 5, pp. 1448-1462, May 2016.

[19] X. Lan, Q. Chen, X. Tang, and L. Cai, "Achievable Rate Region of the Buffer-Aided Two-Way Energy Harvesting Relay Network," *IEEE Trans. on Vehicular Tech.*, vol. 67, no. 11, pp. 11127-11142, Nov. 2018.

[20] I. Krikidis, S. Timotheou, and S. Sasaki, "RF Energy Transfer for Cooperative Networks: Data Relaying or Energy Harvesting?," *IEEE Commun. Letters*, vol. 16, no. 11, pp. 1772-1775, Nov. 2012.

[21] X. Lu, P. Wang, D. Niyato, D. I. Kim, and Z. Han, "Wireless Networks With RF Energy Harvesting: A Contemporary Survey," *IEEE Commun. Surveys & Tutorials*, vol. 17, no. 2, pp. 757-789, 2015.
[22] M. J. Neely, *Stochastic Network Optimization with Application to Communication and queueing systems*, Morgan and Claypool, 2010.
[23] H. Takagi, *Queueing Analysis: Discrete-time systems*, 1993.
[24] F. Farhadi and F. Ashtiani, "Stability Region of a Slotted Aloha Network with K-Exponential Backoff," https://arxiv.org/abs/1406.4448.
[25] L. Shi, Y. Ye, R. Q. Hu, and H. Zhang, "System Outage Performance for Three-Step Two-Way Energy Harvesting DF Relaying," in *IEEE Trans. on Vehicular Tech.*, vol. 68, no. 4, pp. 3600-3612, April 2019.
[26] M. Moradian, F. Ashtiani, and Y. J. Zhang, "Optimal Relaying in Energy Harvesting Wireless Networks with Wireless-Powered Relays," in *IEEE Trans. Green Commun. Net.*, vol. 3, no. 4, pp. 1072-1086, Dec. 2019.
[27] G. latouche and V. Ramaswami, *Introduction to Matrix Analytic Methods in Stochastic Modeling*, 1999.
[28] L. Kleinrock, *Queueing Systems*, vol. I, II, John Wiley and Sons, 1975.